PIXEL SENSOR MODULE ASSEMBLY PROCEDURES FOR THE CMS HIGH LUMINOSITY LHC UPGRADE

A Thesis

Submitted to the Faculty

of

Purdue University

by

Simran S. Gurdasani

In Partial Fulfillment of the

Requirements for the Degree

of

Master of Science in Physics

December 2020

Purdue University

West Lafayette, Indiana

THE PURDUE UNIVERSITY GRADUATE SCHOOL
STATEMENT OF THESIS APPROVAL

Dr. Matthew Jones, Chair

Department of Physics

Dr. Andreas Jung

Department of Physics

Dr. Rafael Lang

Department of Physics

Approved by:

Dr. John Finley

Head of the School Graduate Program

ACKNOWLEDGMENTS

At the very onset of this report, I would like to acknowledge the support I received from the CMS group at Purdue University located in West Lafayette, IN, USA. I would like to thank Prof. Matthew Jones for providing me the opportunity to be involved in this project and my masters thesis committee for providing their time and expertise in examining this work. The material presented in this thesis is based upon work supported by the U.S. Department of Energy, Office of Science, High Energy Physics program under Award Number DE-SC0007884.

This thesis would not be possible without the added support of Prof. Andreas Jung, Dr. Souvik Das and Dr. Ridhi Chawla. I would like to thank Dr. Caleb Fangmeier for getting me up to speed with his previously designed software framework at University of Nebraska, Lincoln, that was adopted for this project. In addition, I would like to acknowledge the work of undergraduates, Berkley Weyer and Surkhab Kaur for their contributions to the experiments discussed in this thesis. The administrative staff at Purdue, especially Ms. Sandy Formica's unending support was also crucial to the completion of this degree.

Finally, I would like to thank my friends and family for their continued support of goal to pursue an academic career in particle physics.

TABLE OF CONTENTS

LIST OF TABLES

LIST OF FIGURES

Figure Page

Figure Page

ABBREVIATIONS

CERN	Conseil Européen pour la Recherche Nucléaire (European Council for Nuclear Research)
LHC	Large Hadron Collider
HL-LHC	High Lumionsity - LHC
CMS	Compact Muon Solenoid
TFPX	Tracker Forward Pixel Detector
P5	LHC Point 5, the location where the CMS detector is installed.
BBM	Bare Bonded Module
ROC	Read Out Chip
CROC	CMS-Readout Chip
PROC	Pixel-Readout Chip
HDI	High Density Interconnect
TBM	Token Bit Manager
CMOS	Complementary Metal Oxide Semiconductor
IC	Integrated Circuit
PCB	Printer Circuit Board
ENEPIG	Electroless Nickel Electroless Palladium Immersion Gold: type of finish for a PCB
GUI	Graphic User Interface

ABSTRACT

Gurdasani, Simran S. M.Sc., Purdue University, December 2020. Pixel Sensor Module Assembly Procedures for the CMS High Luminosity LHC Upgrade. Major Professor: M. Jones, Professor.

The high luminosity phase of the LHC, poised to start taking data in 2027, aims to increase the instantaneous luminosity of the machine to $7.5 \times 10^{34}\,\mathrm{cm}^{-2}\mathrm{s}^{-1}$. This will make it possible for experiments at CERN to make higher precision measurements on known physics phenomenon as well as to search for "new physics". However, this motivates the need for hardware upgrades at the various experiments in order to ensure compatibility with the HL-LHC. This thesis describes some of the efforts to upgrade the inner-most layers of the Compact Muon Solenoid, namely the CMS silicon pixel tracking detector.

Silicon sensors used to track particles are installed in the detector as part of a pixel sensor module. Modules consist of a silicon sensor-readout chip assembly that is wire-bonded to an HDI, or High Density Interconnects to provide power and signals. As part of the upgrade, 2,541 modules need to be assembled delicately and identically with alignment error margins as low as 10 microns. Assembly will be across three production sites in clean rooms to avoid dust and humidity contamination. In addition, the modules need to survive high magnetic fields and extended close-range radiation as part of the HL-LHC [1].

In line with this effort, new materials and assembly procedures able to sustain such damage are investigated. Techniques to assemble modules are explored, specifically precision placing of parts with a robotic gantry and techniques to protect wirebonds. This is followed by a discussion of the accuracy and repeatability.

1. INTRODUCTION

Particle physics aims to answer some of the most fundamental physics questions. Colliders are a very important tool that help physicists in this pursuit. High energy collisions provide a unique insight into fundamental particles that make up the universe and have historically reinforced and helped confirm the accuracy of the standard model. In addition, colliders are also able to extend our physics reach beyond the standard model to explore fundamental questions that have not been answered yet like the matter-antimatter asymmetry, Higgs generation, and super-symmetry amongst many others. This chapter aims to give an overview of the CMS experiment at CERN that seeks to answer some of these fundamental particle physics questions.

1.1 CERN

CERN is one of the largest scientific organizations worldwide that aims to unite intelligent minds across borders with a common goal of furthering science. Founded in 1954, in addition to studying fundamental physics, it has contributed to many technologies like the world wide web that have changed the landscape of every-day life. CERN has been home to various accelerators designed with different goals and increasing in size, energy and complexity. The latest, largest and most powerful of which is the Large Hadron Collider or LHC.

1.2 The Large Hadron Collider

The LHC consists of a ring of super-conducting magnets with diameter 27 km that is located 100 m below ground at the Franco-Swiss border [2]. It is designed to accelerate protons to near the speed of light in two separate tunnels in opposite

directions. It then uses focusing magnets to collide two accelerated beams head-on. The machine has a design capability of colliding proton beams (p-p) at a maximum center-of-mass energy of 14 TeV. In addition, it can collide beams of lead ions (Pb-Pb) at a beam energy of 2.76 TeV/nucleon yielding a total center-of-mass energy of 1.15 PeV as well as proton-lead (p-Pb) collisions.

These beams are made to collide at four different points along the LHC ring, each of which is equipped with a different detector as shown in Figure 1.1. The largest ones are CMS and ATLAS which are general purpose detectors designed to study all kinds of particles. There are two such detectors by design in order to confirm across experiments any new discoveries that are made. The other two interaction points are occupied by LHCb, to study b-physics, and ALICE, to study quark-gluon plasma physics.

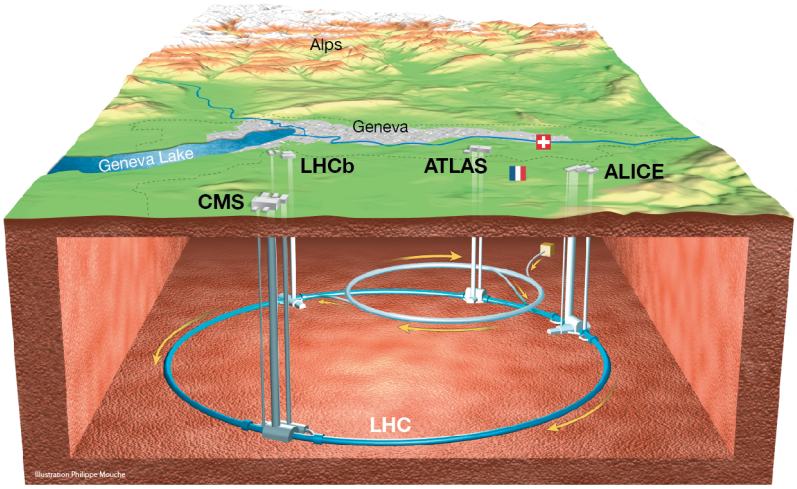

Figure 1.1. LHC underground schematic with the four major experiments: CMS, ATLAS, ALICE and LHCb.

In addition, the LHC has three more smaller experiments called TOTEM, LHCf and MoEDAL. TOTEM and LHCf study "forward particles" which comprise the protons/heavy ions that fail to collide and brush past each other at the intended

interaction point. MoEDAL on the other hand is designed with the aim of detecting the hypothetical monopole.

1.3 The CMS Experiment

This thesis comprises work done to upgrade part of the CMS detector. [3]. The CMS magnet weighs 12,000 tonnes and provides a magnetic field of 4 T.

When protons collide at such high energy, they produce various fundamental particles. The CMS detector is designed to surround the interaction point, or the point at which beams collide, and take a "picture" of what comes out of a collision. Hence, the CMS detector works as a giant, high-speed camera, taking 3D photographs of particle collisions from all directions up to 40 million times each second to produce pictures that can be visualised as in Figure 1.2.

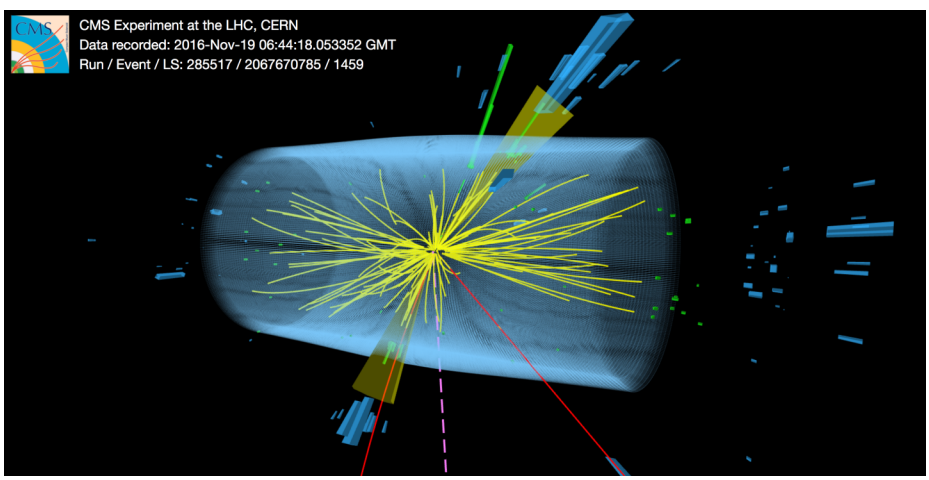

Figure 1.2. An event where a candidate top and antitiop quark were produced. From the top decays there are two b-jet candidates (given by the cones), a muon (the isolated red line), an electron (the green line and green tower), and missing energy (the dotted line).

The trajectories of stable sub-atomic particles produced in collisions, can be differentiated from one another because of the high granularity of the detector. In addition, detectors are designed in layers such that a they interact differently with

different particles. Figure 1.3 shows a transverse slice of CMS and the how tracks of muons, electrons, charged and neutral hadrons and photons can be differentiated from one another.

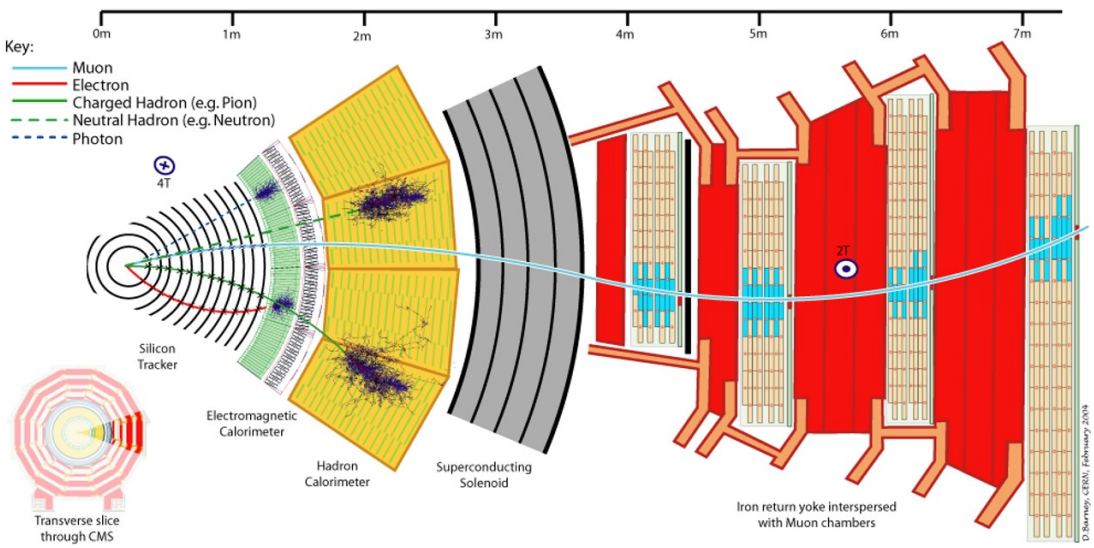

Figure 1.3. Transverse Slice of CMS showing particle detection. Charged particles follow curved paths as opposed to neutral particles. The silicon tracker aims to leave particle paths unimpeded. The calorimeters force particles to decay. Muons travel the farthest.

1. **Silicon Tracker** - This component consists of silicon sensors that record the position of particles at multiple points along their path. These "hits" are then used to reconstruct the path. The tracker is designed to be lightweight so as to minimize any interference with the particles.

2. **Calorimeters** - As opposed to the tracker, calorimeters are designed to measure the energy of particles by forcing them to stop along their path. The Electronic Calorimeter (ECAL) stops electrons and photons while the Hadronic Calorimeter (HCAL) stops hadrons that are made of quarks and gluons.

3. **Superconducting Solenoid** - The tracker and calorimeters sit within the aforementioned superconducting magnet that provides a 4 T magnetic field.

The lorentz force provided by this magnetic field causes particles to move on a helical trajectory relative to the mass, energy and charge of the particle. Thus tracing the path of a particle gives us a measure of its momentum.

4. **Muon Detector** - As is apparent from the name of the detector, detecting muons is an extremely important task of this detector. Muons are minimum ionizing particles that do not interact hadronically. They are leptons like electrons and positrons but weigh about 200 times as much as an electron. Therefore muons penetrate the CMS detector to the outermost layers where they are detected by gas-ionization chambers.

1.3.1 Silicon Pixel Detector

The silicon pixel detector is composed of the outer tracker made of silicon strip detectors, and the inner tracker made of silicon pixel detectors. This section provides an overview of the current design and capabilities of the inner pixel detector.

The silicon pixel detector is located closest to the interaction point and hence, is hit with the highest density of particles and maximum radiation. It consists of the barrel pixel region (BPIX): 4 concentric layers and the forward pixel region (FPIX): 6 transverse layers with a turbine-blade like geometry, 3 on each end of the barrel region further detailed in Table 1.1 and represented pictorially in Figure 1.4.

Table 1.1.
Components of the Silicon Pixel Detector

Region	**Location and Size**	**# Modules**	**# Pixels**
Barrel	r = 2.9, 6.8, 10.9, 16.0 cm length in z = 55 cm	1184	79M
Pixel	z = ± 29.1 ± 39.6 ± 51.6 cm range in r = 4.5 to 16.1 cm	672	45M

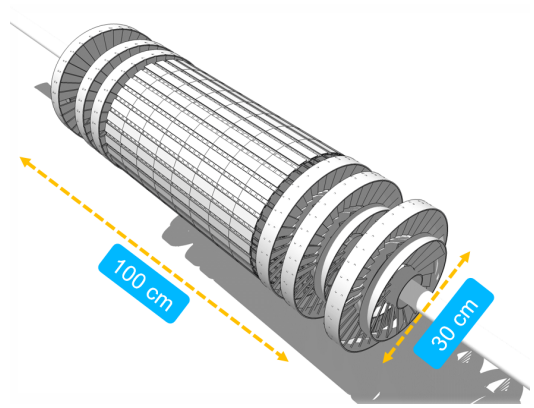

Figure 1.4. Current layout of BPIX and FPIX in the CMS detector: Phase-I upgrade design of the detector.

The forward and barrel layers together provide four-hit coverage for all tracks in an η range of $\pm 2\,5$. In general, pseudo-rapidity [4] is defined in equation 1.1

$$\eta = -\log \tan \frac{\theta}{2} \tag{1.1}$$

where θ is the angle between the particle three-momentum $\mathbf{p}$ and the positive direction of the beam axis. Hence, a particle perfectly in the transverse plane and $\theta = 90$ gives us an $\eta = 0$ while $\theta = 0$ gives an $\eta = \pm\infty$. It then follows that the eta coverage of a detector at the LHC shows how effectively particles with a trajectory almost parallel to the beam axis can be detected as is shown in Figure 1.5.

Another parameter of the LHC that is relevant in describing the working of the silicon detector is pile-up. Because collisions in the LHC are of bunches of protons rather than single protons, each bunch crossing in fact has more than one collision; called pile-up. This means that the tracks originating from an event point back to more than one collision point. The silicon tracker's resolution plays an important role in differentiating these tracks. It is crucial in identifying tracks that come from the primary interaction vertex and discarding tracks that come from pile-up vertices.

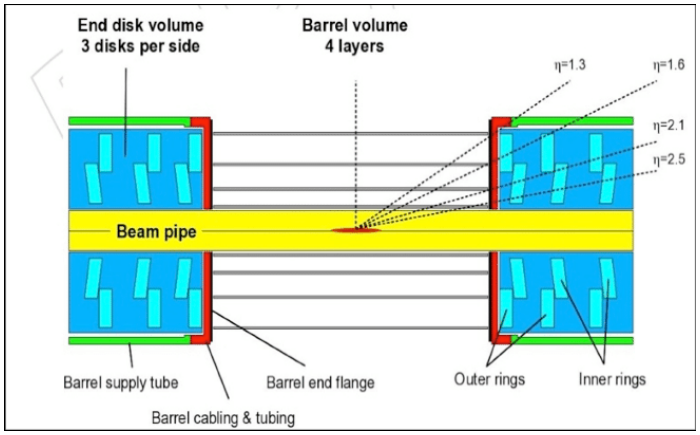

Figure 1.5. Eta coverage of the current CMS pixel detector

1.4 High Luminosity-LHC

Luminosity is a measure of the number of collisions that can be produced in a detector per cm^2 per s. With a higher number of collisions, more data is collected leading to better statistics for high precision measurements as well as increased production of rare events leading to more efficient "new physics" searches. At nominal luminosity the LHC produced 10^{34} proton collisions per cm^2 per s. It is currently operating at twice that luminosity and a planned luminosity of 5 to $7.5 \times 10^{34}\,\mathrm{cm}^{-2}\mathrm{s}^{-1}$ will be achieved as part of what is called the High Luminosity era of the LHC. The timeline of increasing energy of collisions and planned luminosity is shown in Figure 1.6.

In addition to more data, HL-LHC brings with it challenging environments that will affect greatly the performance of the tracking detector including higher pile-up. The LHC recorded an average of 32 pile-up events in 2017-18 which is expected to go up to 140-200 during the HL-LHC. This can be pictorially represented as in Figure 1.7 showing a high pile-up event with 78 reconstructed vertices. Number of hits increase linearly with pile-up. However, track reconstruction relies on using hit combinatorics to accurately reconstruct these tracks. As the number of hits increase

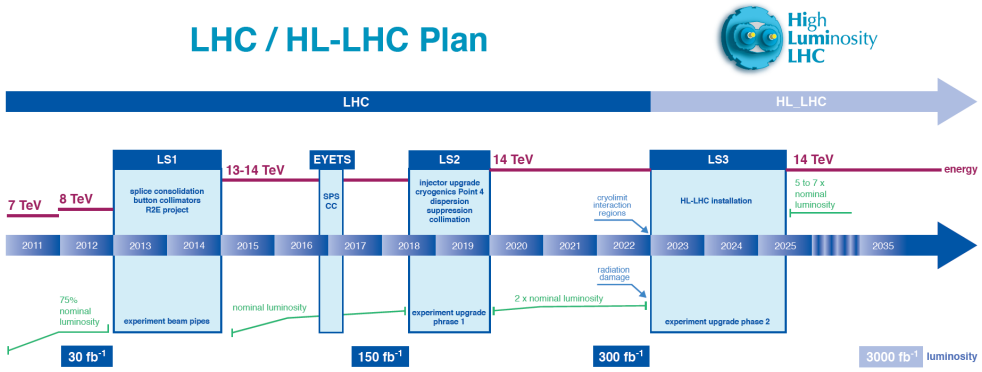

Figure 1.6. Timeline of the high luminosity LHC showing luminosity and center of mass energy upgrades from 2011 till 2035.

linearly, the combinations of possible tracks increase much faster than linearly. Thus, track resolution in the HL-LHC environment requires a much more granular and efficient tracker.

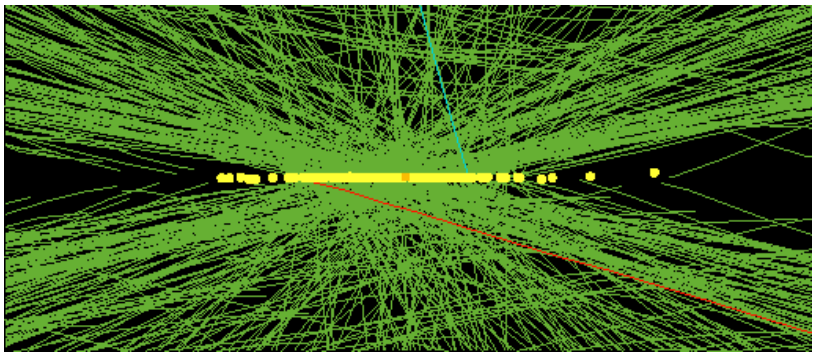

Figure 1.7. High pile-up event with 78 reconstructed vertices.

This high collision rate means that the inner-most layer of the tracker will be exposed to a total ionising dose of 1.2 Grad and $2.3 \times 10^{16}\,\mathrm{n_{eq}cm^{-2}}$ requiring much higher radiation hardness [1]. A study of all the source of radiation and calculation of these expectations is discussed in [5].

2. MOTIVATION

2.1 Phase II Upgrade

The Phase-I pixel detector, installed in 2017, was designed for the current luminosity of $1 \times 10^{34}\,\mathrm{cm}^{-2}\mathrm{s}^{-1}$ and to withstand the LHC radiation over a 10 year period (2017-2027) with the option of replacing damaged elements during regular shutdowns. The Phase-II tracker will need to keep the above accessibility and have higher granularity to distinguish the higher density of particle tracks produced by more collisions described previously. Overall radiation hardness needs to be greatly improved to withstand unprecedented levels of radiation as explained in section 1.4. In short, to account for an expected integrated luminosity of $3000\,\mathrm{fb}^{-1}$, 140-200 pile-up events, a total ionising dose of 1.2 Grad and $2.3 \times 10^{16}\,\mathrm{n_{eq}cm}^{-2}$. The material present in the detector needs to be reduced to improve overall track reconstruction by reducing interaction with the particles before they reach the calorimeters and further into the detector.

The Phase I detector discussed previously had 4 barrel layers and three forward layers. The planned Phase II detector will have 4 barrel, 8 forward and 4 endcap layers as shown in Figure 2.1. TEPX or the Endcap region will be a new addition to the pixel detector in addition to a much longer forward pixel detector.

The extended length of the pixel detector will also greatly increase to incorporate values up to $\eta = \pm 4$ as opposed to the current $\eta = \pm 2\,5$ This will increase the active surface of the detector to $4\,\mathrm{m}^2$ from the current value of $2.7\,\mathrm{m}^2$

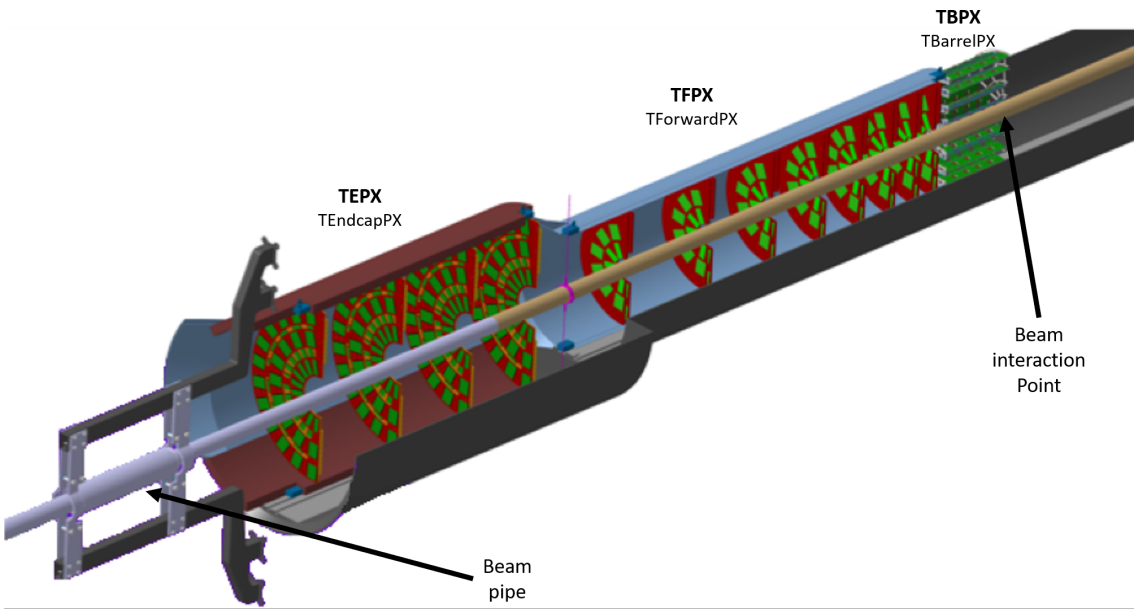

Figure 2.1. Schematic of the Phase II pixel detector showing the barrel pixel layers closest to the beam interaction point, followed by 8 forward and 4 endcap layers.

2.2 Pixel Sensor Modules

A pixel sensor module that is installed into the CMS inner tracker consists of a flex circuit glued and wire-bonded to a silicon sensor with read out chip. The flex-circuit is called a high density interconnect or HDI that collects data, provides clock, trigger, control and power signals amongst other passive and active design components to the sensor. Silicon atoms provide the ionizing medium, or the matter with which incident particles interact. The interaction can then be read out using a readout chip, specifically C-ROC or CMS-readout chip. The silicon sensor along with C-ROC is called a sensor-ROC assembly, the working of which is explained in Section 2.2.1. Figure 2.2 shows the simplified anatomy of the current assembled module version in CMS. A layer of epoxy is placed between the HDI and sensor to facilitate wire-bonding and provide an some more stiffness to the sensor.

Phase I used the PSI46 design for the C-ROC build with 250 nm CMOS technology. CMOS or Complementary Metal Oxide Semiconductor technology is a method used to produce integrated circuits. This required a TBM or token bit manager to order and communicate the hits that are read out from an active pixel region as shown in Figure 2.2.

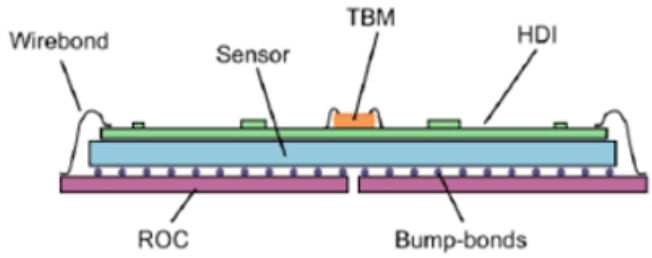

Figure 2.2. Simplified anatomy of an assembled pixel module currently installed in the CMS inner tracker (Phase-1).

2.2.1 The working of a sensor-ROC assembly

Silicon, apart from being abundantly available and easily produced in crystal or wafer configuration (thanks to its extensive use in modern day electronics), has the advantage that it is much denser than gas. This is advantageous because particles are detected by their interaction with detector material, hence, semiconductor ionization chambers can detect particles in a much smaller volume than gas ionization chambers.

When an incident charged particle traverses through the depleted region of a silicon p-n junction, it ionizes the medium creating e-h pairs as shown in Figure 2.3. The incident particle consequently loses energy and slows down in the process. The semiconductor detector functions as an ionization chamber. Under an applied electric field, the electrons and holes drift inside the silicon lattice and then can be collected at electrodes.

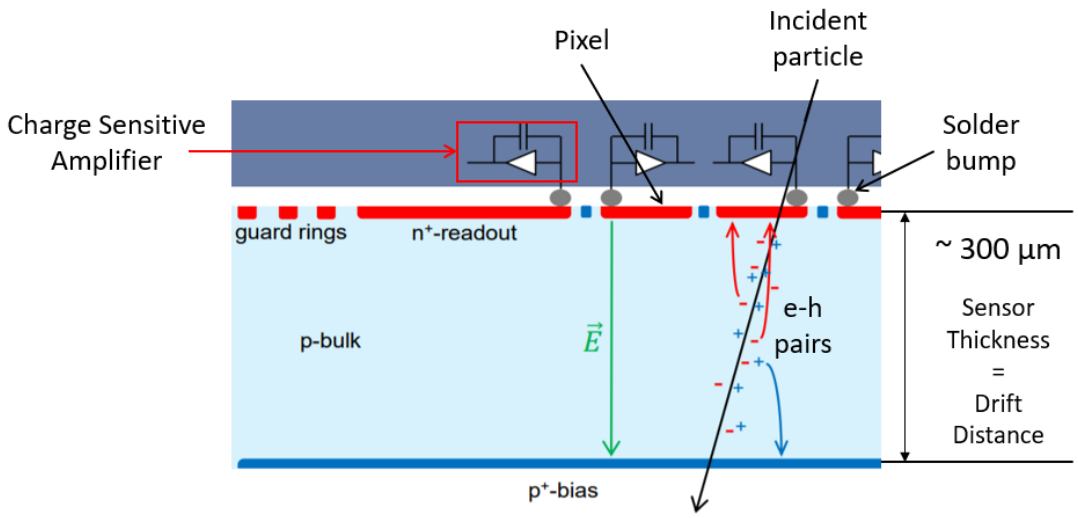

Figure 2.3. Particle detection in planar n-in-p silicon sensor. The incident charged particle creates e-h pairs as it traverses the sensor thickness. This is the drift distance that the e-h pairs have to travel to be detected at the electrodes. The charge sensitive amplifier (CSA) provides a measure of the sensor current integral by giving an output voltage signal proportional to the amount of charge collected from the sensor. [6]

The number of e-h pairs produced depends on the energy deposited by the incident particle. This is characterized by the Bethe-Bloch formula (2.1) which describes that the energy depends on the momentum of the incident particle but as well as the properties of the medium traversed.

$$-\left\langle \frac{dE}{dx} \right\rangle = \frac{4\pi}{m_e c^2} \cdot \frac{nz^2}{\beta^2} \cdot \left(\frac{e^2}{4\pi\varepsilon_0} \right)^2 \cdot \left[\ln\left(\frac{2m_e c^2 \beta^2}{I \cdot (1-\beta^2)} \right) - \beta^2 \right] \tag{2.1}$$

Equation 2.1 describes the energy deposition per unit length for a particle with speed v, charge z (in multiples of the electron charge), and energy E, traveling a distance x into a target of electron number density n and mean excitation potential I. c is the speed of light and ϵ_0 the vacuum permittivity, $\beta = \frac{\mathrm{v}}{\mathrm{c}}$, e and $\mathrm{m_e}$ the electron charge and rest mass respectively. It is clear from this formula that the charge detected due

an incident charged particle does not relate trivially to the mass or energy of the incident particle.

As an example, let's consider a minumum ioinizing particle or MIP traversing a $\sim 300\,\mu$m sensor as is standard in CMS. The mean loss of energy of a MIP in $1\,\mu$m of silicon is 388 eV. The energy required to generate an e-h pair in silicon is 3.6 eV. Therefore, a MIP traversing through a $300\,\mu$m silicon sensor produces, on average, 33,000 e-h pairs. This corresponds to a 5.2 fC of charge. If the silicon sensor can detect a minimum of 5.2 fC of charge, an incident particle can be detected. This provides the threshold of charge that needs to be read out by the pixel sensor.

In order to increase position accuracy, the silicon sensor used in CMS is a hybrid pixel detector which entails dividing the electrodes on the silicon sensor into a rectangular array and connecting each pixel to its own electronics channel on the readout chip (ROC) using a solder bump bond as shown in Figure 2.4.

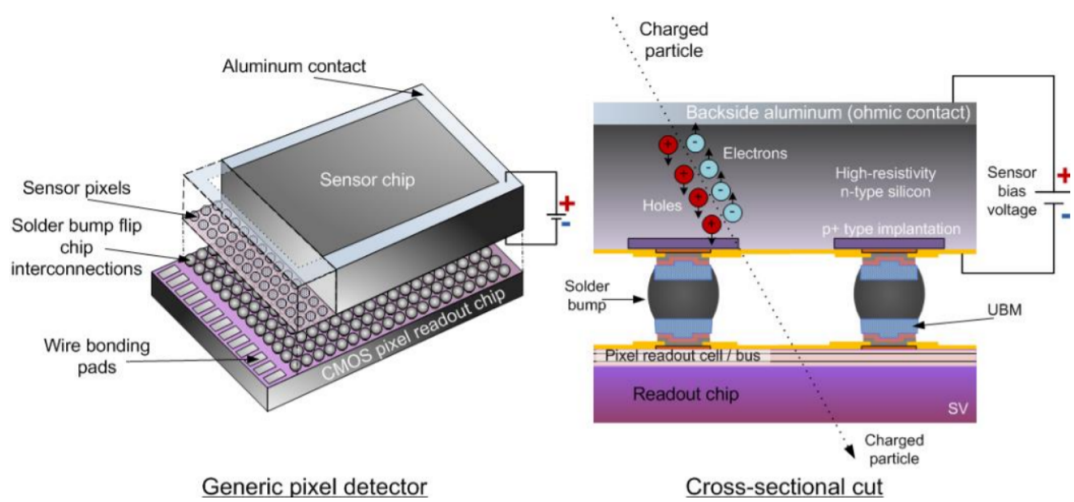

Figure 2.4. Layout of a hybrid pixel detector used to increase position accuracy in the CMS tracker.

More generically, electrons and holes are collected at electrodes that can be segmented as pixels or strips or pads. For a silicon pixel sensor, it follows then that

smaller the pixel, the more precisely a particle hit position can be resolved. Each pixel in the rectangular array of pixels is set to have a binary output, The current size of a pixels in CMS is $100\,\mu$m $\times$ $150\,\mu$m.

Electrons also travel much faster than, for example, gas ions. This ensures a collection time of e-h pairs generated by an incident particle to be in the order of nanoseconds. Hence, making it possible to have subsequent collisions very quickly.

While for the Phase-II upgrade, we refer to the sensor bump-bonded to the readout chip component explained above as a sensor-ROC assembly. Previous documentation may refer to these as Bump-Bonded-Modules, BBMs or bare modules as these were the terms used in the Phase-I upgrade.

2.3 Upgraded Phase-II module design

There will be two types of modules used in this upgrade as depicted in Figure 2.5: 1×2 modules with two read out chips and 2×2 modules with four read out chips. The new pixel size will be $25\,\mu$m $\times$ $100\,\mu$m or $50\,\mu$m $\times$ $50\,\mu$m as opposed to the Phase I size of $100\,\mu$m $\times$ $150\,\mu$m.

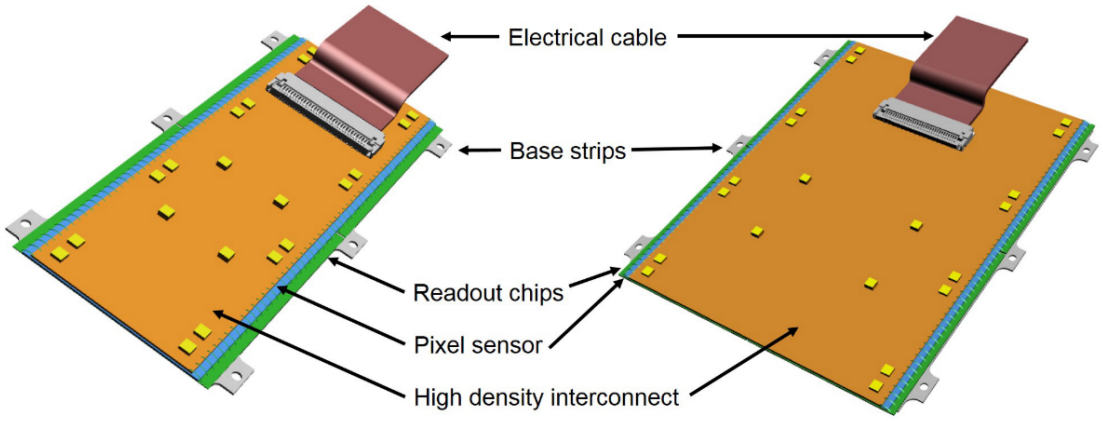

Figure 2.5. CAD drawing of 1 x 2 and 2 x 2 modules [7]

The Phase II C-ROC will be a RD53A chip produced as a joint CMS-ATLAS RD53 collaboration. This is produced using 65 nm CMOS technology which is compatible with smaller pixel sizes. A review of the developments of readout chips and advantages of newer CMOS technologies is provided in [8]. The size of the sensor will be thinner, within 100-150 μm. Thinner sensors are more compatible with higher particle fluences and radiation. In addition, for Phase II, it is decided to have n-in-p planar sensors as well as 3D sensors to be compatible with HL-LHC environments. The Phase-2 Upgrade of the CMS Tracker - Technical Design Report [7] gives a comprehensive review of studies done to conclude the above design specifications.

2.3.1 Module assembly challenges

The assembled module for Phase-II has similar anatomy to Phase-I with the absence of TBM chip as is shown in Figure 2.6. The size, performance and technology used to produce the components will be in line with HL-LHC requirements. However, this means that module assembly for Phase-II brings with it the following challenges:

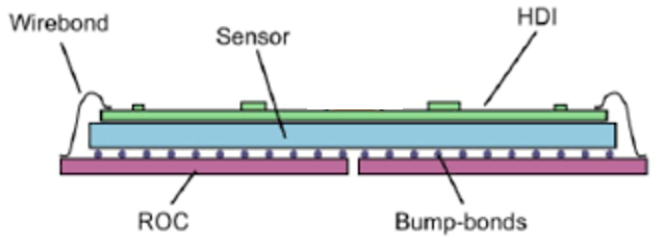

Figure 2.6. Simplified anatomy of an assembled pixel module to be installed in the CMS inner tracker (Phase-II).

1. Exploration of scalable procedures to handle different module sizes and designs.

2. Means to assemble 2541 modules in 3 years.

3. Wire-bonding at a more intricate pitch. - Wire-bonds form the communication channels between HDI and sensor-ROC assembly and as granularity of the modules increases, higher density of connections is required.

4. Protection of wire bonds from mechanical damage, radiation and other environmental effects.

5. Development of new procedures to coat surfaces or parts of the module that are more prone to radiation damage.

   - Irradiation tests on all components that go into assembly as well as on fully assembled modules.
   - Materials must remain intact after radiation of 1 GRad

6. Modules must be fully assembled and tested prior to mounting on disks

   - Testing and quality assurance procedures for new modules need to be established.
   - Modules must be stressed to catch infant mortality.

3. EXPERIMENTAL WORK

Production for the CMS Phase-II Silicon Tracking Forward Pixel Detector will be spread across three institutions. Responsibilities include development of sensors and ROC, assembly of modules, electronics, mechanics and finally assembly of the detector [7]. At the module assembly factories, which include Purdue University, University of Nebraska, Lincoln and Catholic University of America, the work-flow showed in Figure 3.1 will be followed during production. This section focuses on development of two out of four required processes: gluing & encapsulation.

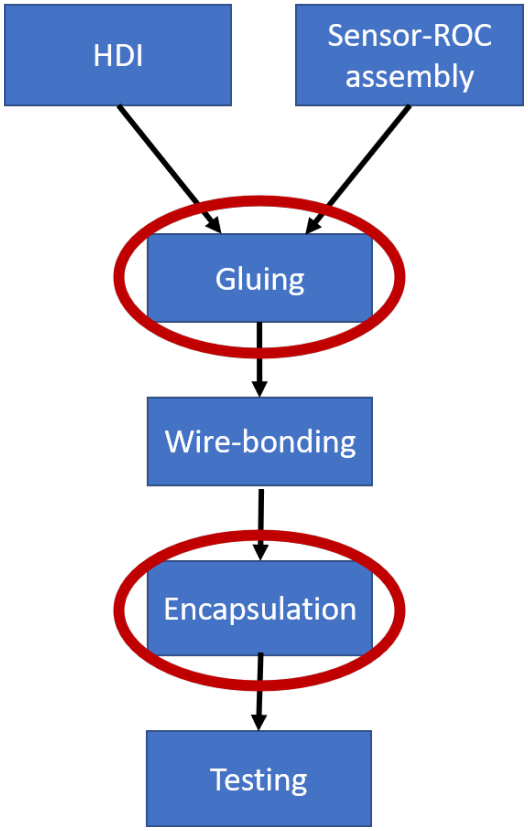

Figure 3.1. Stages of assembly

3.1 Mock-Module Assembly

In order to establish methods for assembly, initially mock-modules are assembled for practice and trials. This includes a glass piece made to model the sensor-ROC assembly and a printed circuit board to model HDI specifications as shown in Figure 3.2. The glass piece has the same geometry expected for 1 x 2 C-ROC modules and heaters fabricated to dissipate the expected heat load and hence called a thermal mock-up. The flex circuit just provides power to the heater elements.

The thermal mock-up is developed at Purdue to be used in mock-modules in place of the very expensive sensor-ROC assemblies. The design evolves to match developments of the sensor-ROC assembly, specifically the design of the RD53A chip designed by the RD53 calibration. A thermal mock-up is made by depositing aluminum on the entire surface of a glass wafer, followed by etching traces to make resistive structures mimicking the pixel array. The version used in thesis has structures attached to most bond pads for powering heaters and electrical continuity measurements.

The HDI is a very thin printed circuit board or PCB with ENEPIG finish. ENEPIG which is an acronym for Electroless Nickel Electroless Palladium Immersion Gold is a type of surface finish used across different PCB assemblies. ENEPIG finishes are used widely in industry as a low cost advantage to gold finishes. It is also the preferred alternative for wire-bonding applications, offering a greater pull strength (aluminum wire: up to 10 gram-force) than soft gold and ENIG (Electroless Nickel Immersion Gold) finishes.

Thermal mock-ups once manufactured, diced and cleaned are stored in a gel pack in dry storage along with HDIs ready to be assembled. Both thermal mock-ups and HDIs have serial number as is shown in Figure 3.3. The thermal mock-ups have serial numbers on the gel pack cover corresponding to their position inside as will be the case for sensor-ROC assemblies. HDIs have serial numbers on them.

Before assembling mock-modules, the thermal mock-ups must first be examined for any design or manufacturing defects. Silicon is not the easiest material to work

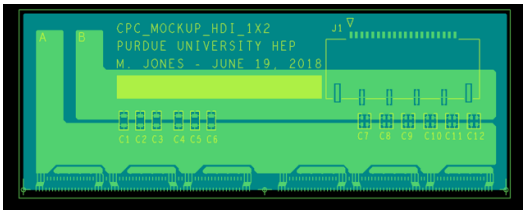

(a) HDI

(b) Thermal Mock-up

Figure 3.2. Design of mock module components

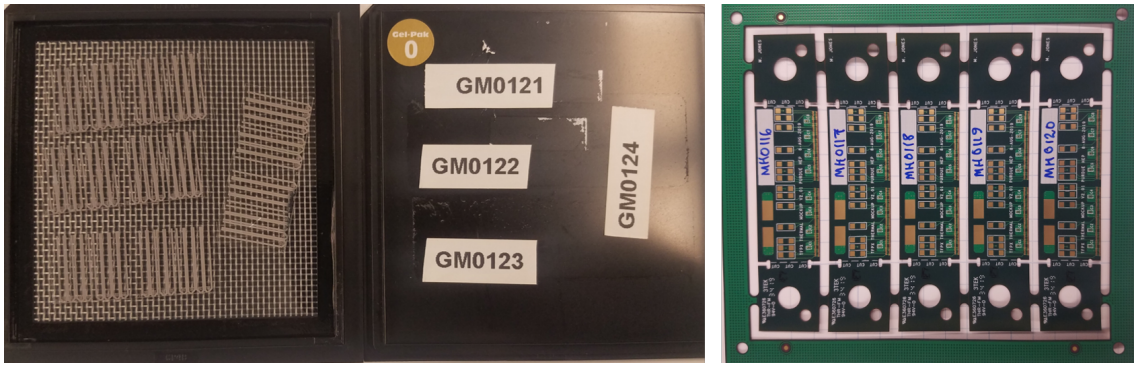

Figure 3.3. Parts of mock-module ready for assembly. Four thermal mock-ups with serial numbers on the left and five HDIs with serial numbers on the right.

with and sensor-ROC assemblies can be contaminated very easily by fingerprints and scratches from rough handling. Hence it is good practice to use a vacuum pen to move them around. While thermal mock-ups are less fragile, the electrical components can also be damaged by scratches. Therefore, it is useful to implement caution when handling thermal mock-ups.

After examination, the HDI and thermal mock-up are glued with a layer of epoxy between them. This provides a layer of radiation protection to the sensors as well as hardened surface below the flex-circuit to allow for the next step of wire-bonding. This is the process where connections called wire-bonds are made between the thermal

mock-up and HDI using Aluminum wire. These bonds then need to be encapsulated with epoxy for protection as is explained in details later in this chapter: 3.4.

Once assembled, the mock modules heat signature can be measured and the wire-bonds can be tested electrically. The module then goes through thermal cycling and irradiation tests that help determine how it will behave in the HL-LHC environment as shown in Figure 3.4.

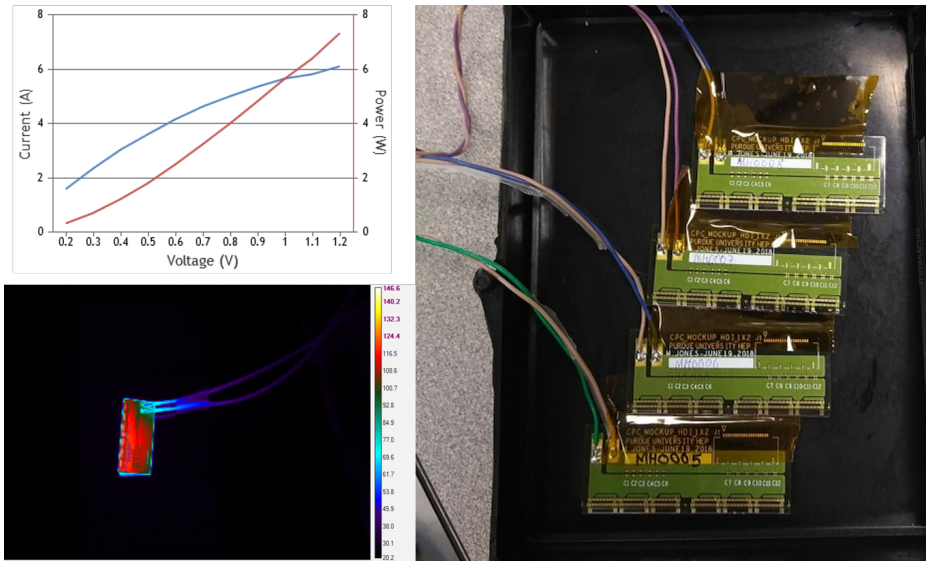

Figure 3.4. Four assembled mock modules along with the electrical test and heat signature of one.

In order to assemble modules repeatedly and precisely, a combination of human commands and robotic machine assembly is developed and described in the subsequent sections.

3.2 Software and Hardware set-up

A github repository is developed with an object-oriented version of Labiew code called pixel-gantry-control (PGC). This framework is adopted from code developed at UNL by Caleb Fangmeier as part of the Phase I production. It is further developed

for R&D at Purdue University and thereafter for Phase II production. The software is designed to support multiple table setups for different assembly factories and to be expandable as production requires adjustments. Standardized software requirements and directions on how to load the software to specific assembly stations are available as part of the forked github repository. [9].

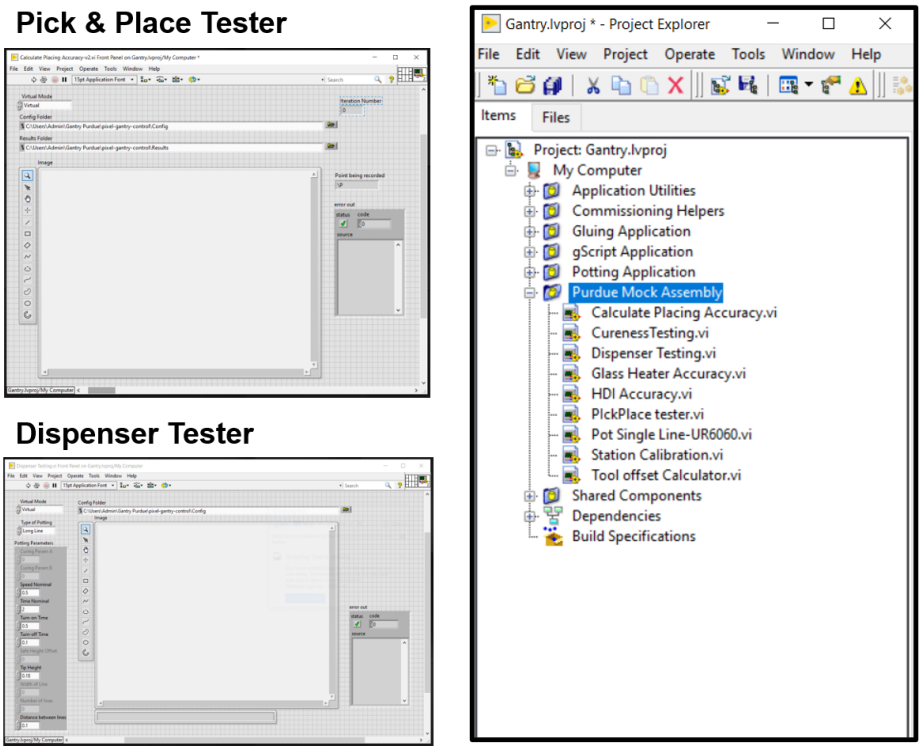

Figure 3.5. Gantry.lvproj it the LabVIEW project consisting of code developed for Phase-II mock module assembly at Purdue on the right. The left shows GUIs of two developed uni-directional workflows to operate the pick and place routine and dispensing routine described in detail in 3.3 and 3.4

LabVIEW is used to interface with four different hardware systems in order to make this assembly possible. While efficient at communicating with different hardware systems simultaneously and providing multiple useful GUIs for users, LabVIEW can be a very memory intensive software. The object-oriented approach which was adopted offers code re-usability and better memory management while keeping com-

munication channels open to all different hardware systems. Complex workflows are designed to have GUIs that facilitate training during module production. They are programmed using unidirectional workflows to provide a clear order of events. This limits the amount of control an operator has but also reduces the ability to cause memory leaks and communication channels to throw errors. Previous iterations of code developed at Purdue had controls to all hardware systems in one GUI. This was more versatile but caused memory leaks and required intensive training. The new process-specific GUIs shown in Figure 3.5 are less busy and facilitate training, which will be beneficial for large scale production.

The four hardware systems used for assembly are now described.

1. **Vacuum manifold** - 32 individual channels to connect vacuum to different assembly stations.

2. **Dispenser System** - the Nordson EFD Ultimas V High Precision Dispenser equipped with a HP7x dispensing tool as shown in Figure 3.6. This provides electronic control of dispense time, pressure, and vacuum settings to accurately and consistently dispense whatever substance is loaded. The Ultimas V consists of most importantly, an intuitive RS232 interface, on which the dispensing pressure is programmed. The HP7x dispensing is a syringe carrier with space to load a 7 cc syringe and a piston controlled by the Ultimus V.

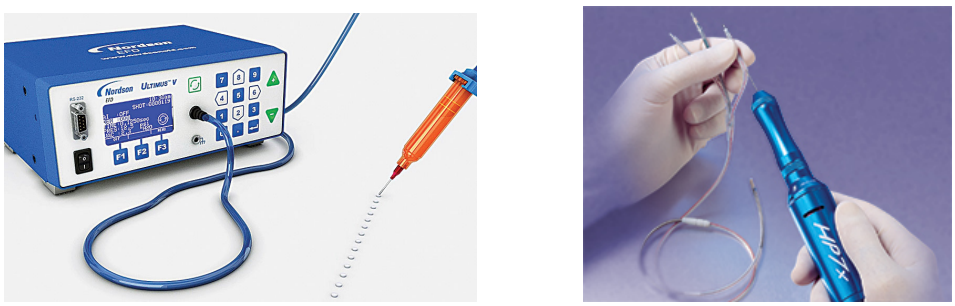

(a) Nordson EFD Ultimas V

(b) HP7x Dispensing Tool

Figure 3.6. Dispenser Tool

3. **Vision System** - consists of a gantry head camera, stand camera and needle calibration cameras. The gantry head camera is an industrial design camera: IDS model UI148xSE. This camera has a field of view of 1.095 mm x0.824 mm with excellent image quality. This thesis uses a resolution of 1920x1080 pixels with a rate of 3.00 fps integrated using a USB 2.0 interface. The stand camera is a generic webcam camera with light attached to a stand with a range of motion enabling different viewing angles. This is essential to developing different stages of assembly. Model: Vimicro USB2.0 UVC PC Camera.

4. **Robotic Gantry** - The Aerotech A3200 Software-Based Machine Controller is used to move the Aerotech AGS10750 gantry positioning system head with ranges of motion in X-Y-Z (750 mm x 750 mm 100 mm) and U which is a 360° rotation in the X-Y plane. The gantry head has a tool holder and a camera attachment as shown in Figure 3.7(a). The tool holder can have different attachments for differing parts of the process. Figure 3.7(b) shows a custom designed tool used for Phase I assembly.

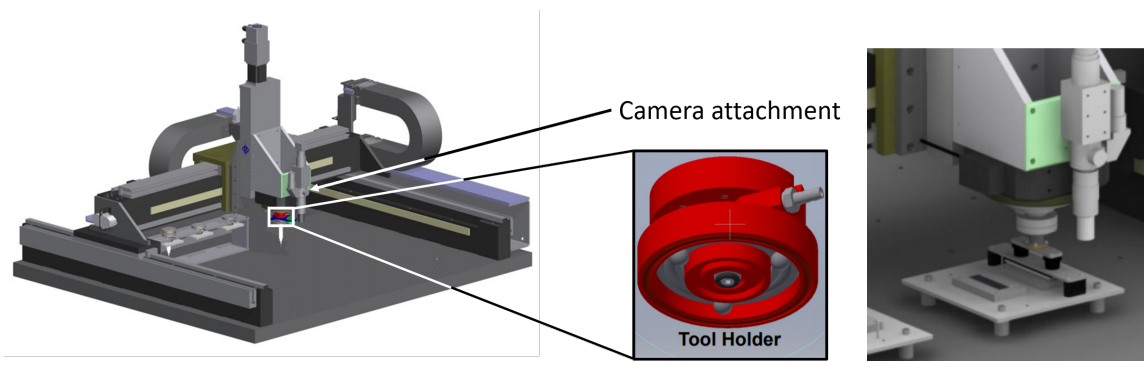

(a) Robotic Gantry with tool holder and camera attachment

(b) Gantry head with attached tool in use

Figure 3.7. Aerotech AGS10750 gantry positioning system with a working space of 750 mm x 750 mm 100 mm

3.3 Gluing Process Development

For the gluing process, the stations used are a launch pad and an assembly station. The launch pad is a chuck on the gantry where the thermal mock-up is placed using a vacuum pen by the operator as shown in Figure 3.8(a). The mock-up is held down by vacuum to be surveyed by the gantry camera before being moved to the assembly station for gluing.

At the assembly station, it is proposed to use an updated mechanical jig with alignments pins for Phase II assembly as shown in Figure 3.8(b). This includes a vacuum table that will be attached to the gantry table firmly and an alignment tool. A module carrier can be placed atop the alignment tool using dowel pins. There is a small, but finite tolerance in the hole size and the alignment pins, so after the module carrier is placed on the pins, it should be pulled towards the operator so that it will systematically be in the same position whenever it is mounted. The alignment tool is screwed to the vacuum table and provides vacuum through the holes in the module carrier to hold the glass mock-up in place.

Alignment of the mock-up is achieved using the robotic gantry. The moving routine which is programmed using LabVIEW code works on the following principle of operation. Once the mock-up is placed on the launch pad under vacuum and surveyed, the pick-up tool makes contact with the mock-up and vacuum is transferred from the launch pad to the pick-up tool. The module is then moved into the pre-determined position on the module carrier and vacuum is transferred from the pick-up tool to the module carrier. The alignment pins provide the reference for alignment of the HDI and the gluing stencil. At this point, if glue is to be applied, the glue stencil is placed on the alignment pins and Araldite 2011 is squeegeed over the holes. The glue stencil is removed and the HDI is placed on the alignment pins, with force applied towards the operator to minimize systematic placement inaccuracies. Then, the gluing weight tool is placed on the alignment pins to apply pressure on the HDI while the glue cures. At first however, placement accuracy measurements are performed without gluing.

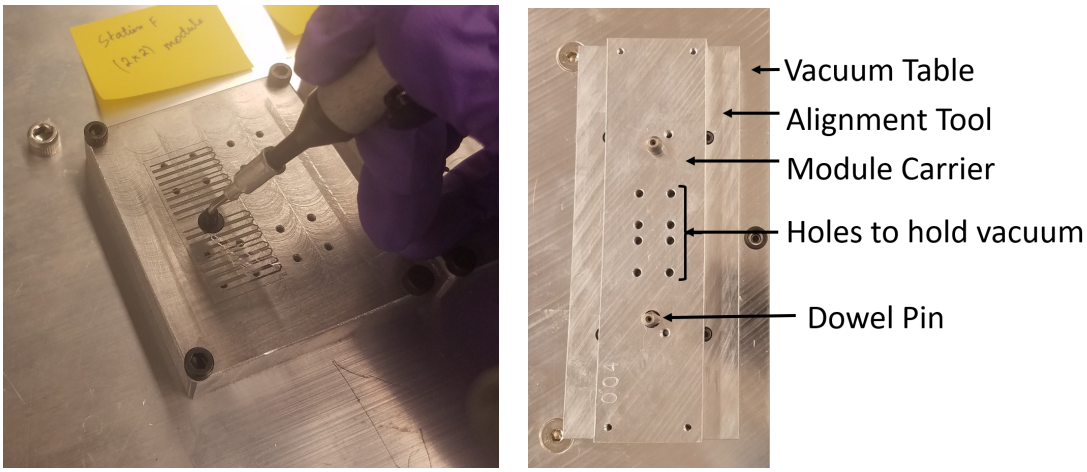

(a) Launch pad to place thermal mock-up with vacuum pen

(b) Assembly station with mechanical pins used for gluing

Figure 3.8. Updated gluing assembly stations for Phase II module assembly at Purdue University

3.3.1 Accuracy Placing Measurements

The HDI and mock-up have to be aligned accurately enough to allow wire-bonding of bond-pads placed at a 100 μm pitch. As is shown in Figure 3.9, the mock-up HDI is placed on top of the mock-heater so that the wire-bonds on the HDI and glass-piece align as required by the process of assembly.

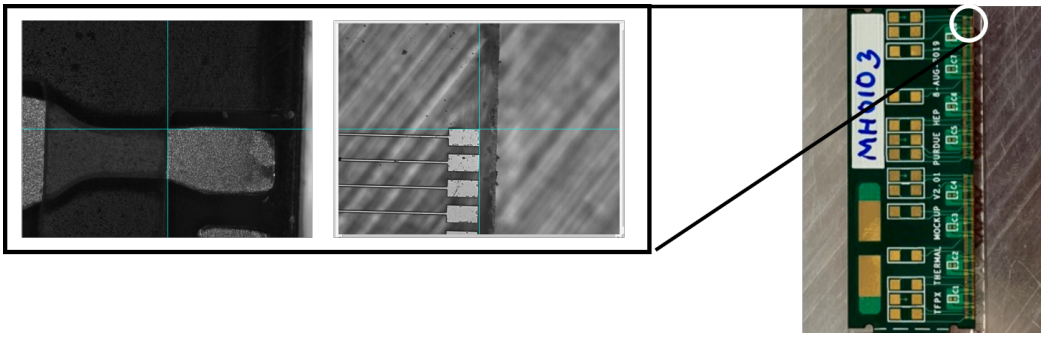

Figure 3.9. Required Alignment of Mock Modules

This section describes the accuracy attained by mechanical pins for the HDI followed by the accuracy attained by the gantry pick and place routine.

Mechanical Pins Accuracy

The HDI design was updated to include extensions that fit over alignment dowel pins. In order to determine the accuracy attained by the mechanical pins, one HDI is placed repeatedly on the assembly station using the alignment pins. It is then pulled toward the operator, and features on the HDI are recorded. The HDI has a row of bond-pads on one edge broken into two sections. The features recorded are corners of the first and last bond-pad in each set of bond-pads as shown in Figure 3.10. The Y direction here is along the length of the HDI and more important as this is the direction error that must be minimized to ensure alignment with the glass piece bond-pads.

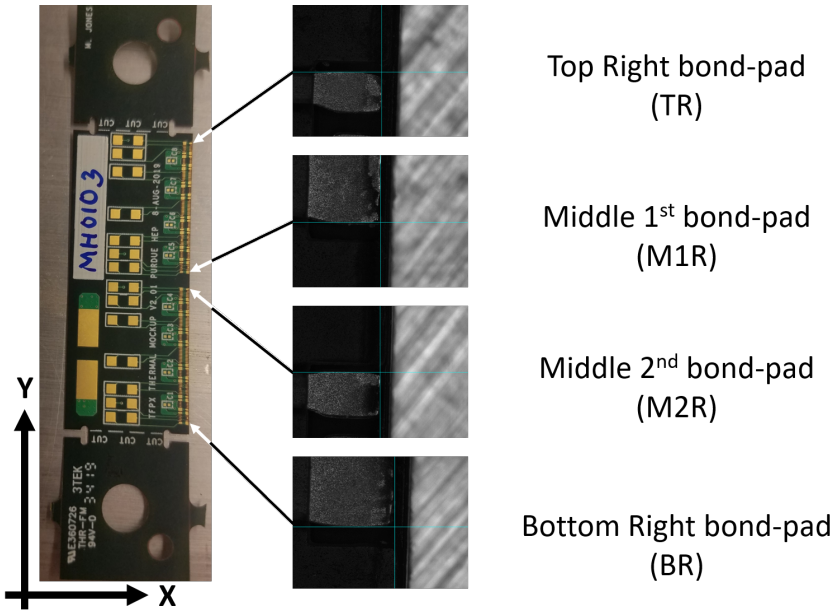

Figure 3.10. The orientation of the coordinate system and features on the HDI that are recorded to calculate placing accuracy. Henceforth these are referred to as as TR, M1R, M2R and BR bond-pads on the HDI

Over multiple iterations, the X and Y gantry coordinates of the corner of a given bond-pad on the HDI is measured. Figure 3.11(a) shows the scatter plot of x and y coordinates of the TR bond-pad followed by histograms showing deviation in x and y separately in 3.11(b) and 3.11(c).

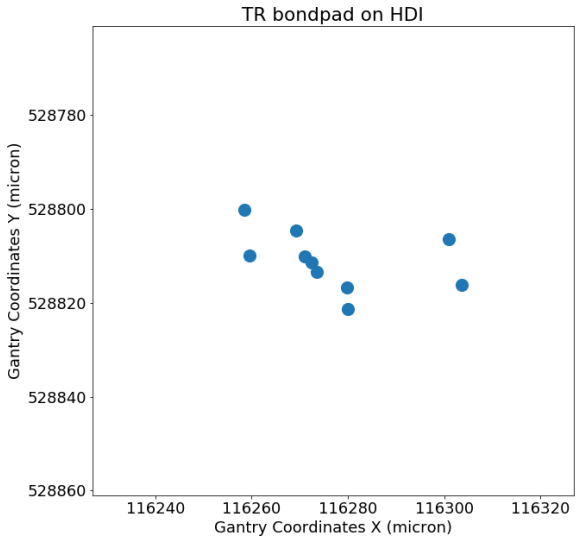

(a) Scatter plot of top right bond-pad on HDI

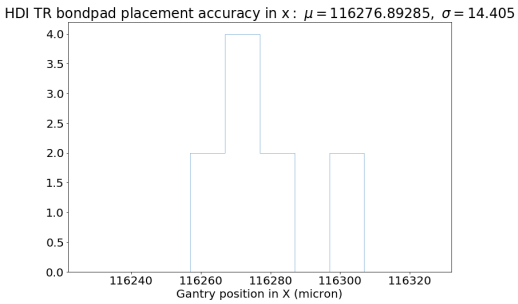

(b) Deviation in X, σ_x =14.405 μm

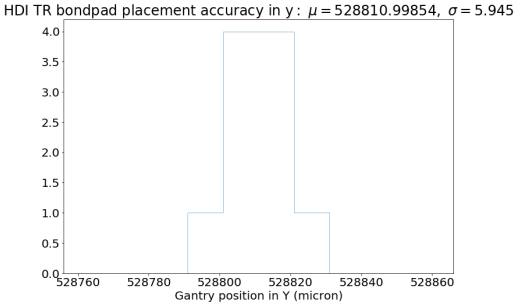

(c) Deviation in Y, σ_y =5.945 μm

Figure 3.11. Spread of the position of top-right bond-pad on HDI over 10 iterations of alignment with mechanical pins.

Figure 3.12 shows the same measurements for the remaining features of the HDI.

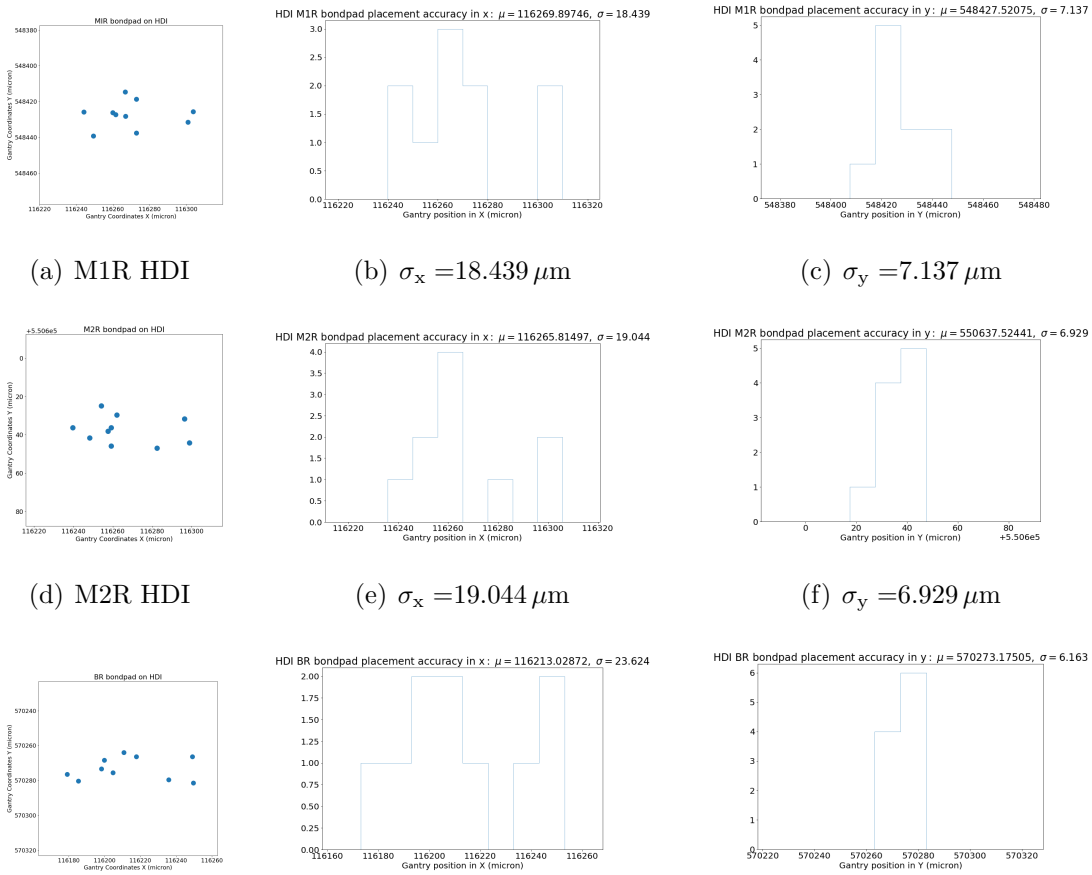

(a) M1R HDI (b) σ_x =18.439 μm (c) σ_y =7.137 μm

(d) M2R HDI (e) σ_x =19.044 μm (f) σ_y =6.929 μm

(g) BR HDI (h) σ_x =23.624 μm (i) σ_y =6.163 μm

Figure 3.12. Spread of the position of M1R, M2R and BR bond-pads on HDI over 10 iterations of alignment with mechanical pins.

The spread in the X and Y direction can perhaps be explained by the fact that the HDI is not held down when placed over the mechanical pins. This could cause it to be not entirely flat. This can be verified by measuring the placement once the HDI is glued or held down by a weight which is yet to be designed. The larger spread in X could account for the fact that the HDI is pulled vertically towards the operator when placed, reducing systematic error in the Y direction. It is considerably harder to pull it in the X direction. In addition the copper etching is not perfect as observed

in the image of the bond-pad in Figure 3.10 causing imperfect edges. It is proposed to include fiducials on the HDIs in future iterations to get more precise measurements.

Gantry Placing Accuracy

Similarly for the mock-up, a pick up tool is used to place the glass mock-up module at a predetermined position such that it aligns with the HDI when placed from above. This process demonstrated in Figure 3.13 starts with manually placing the thermal mock-up on the 'launch pad'.

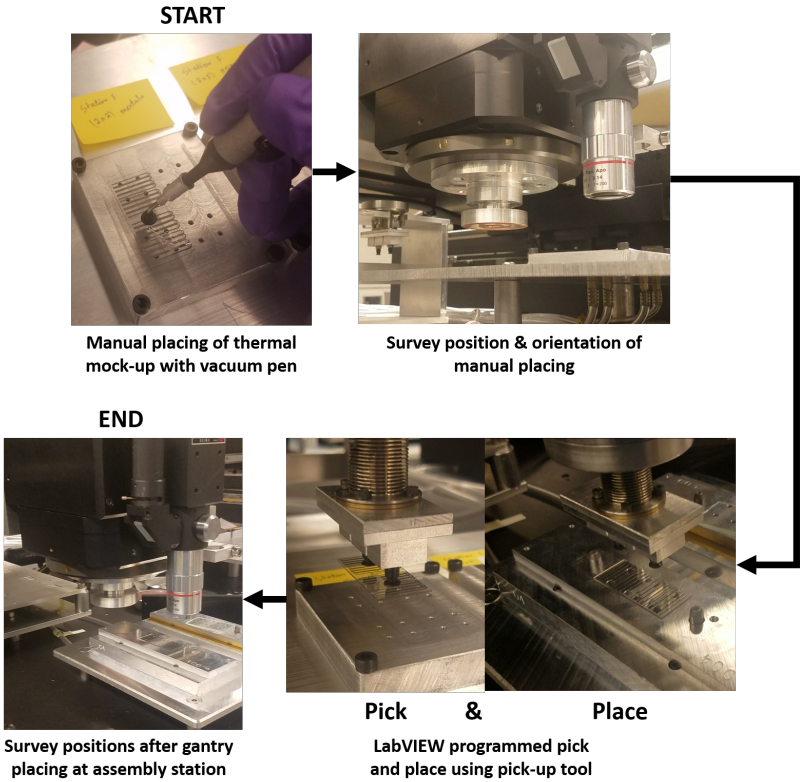

Figure 3.13. The pick and place process for placement accuracy measurements.

Then, using the camera attachment on the gantry head the configuration in with the thermal mock-up is placed is inspected. The gantry head then employs the pick-

up tool to align itself in position and orientation with the manually placed thermal mock-up. It then corrects the rotation to be perfectly aligned with the gantry table axes and brings the glass piece over to the assembly station. For placement accuracy measurements, after placement of thermal mock-up on the alignment station the tool is returned and the camera attachment proceeds to survey features on the glass piece.

The process is iterated and the location of the four fiducials shown in Figure 3.14 measured.

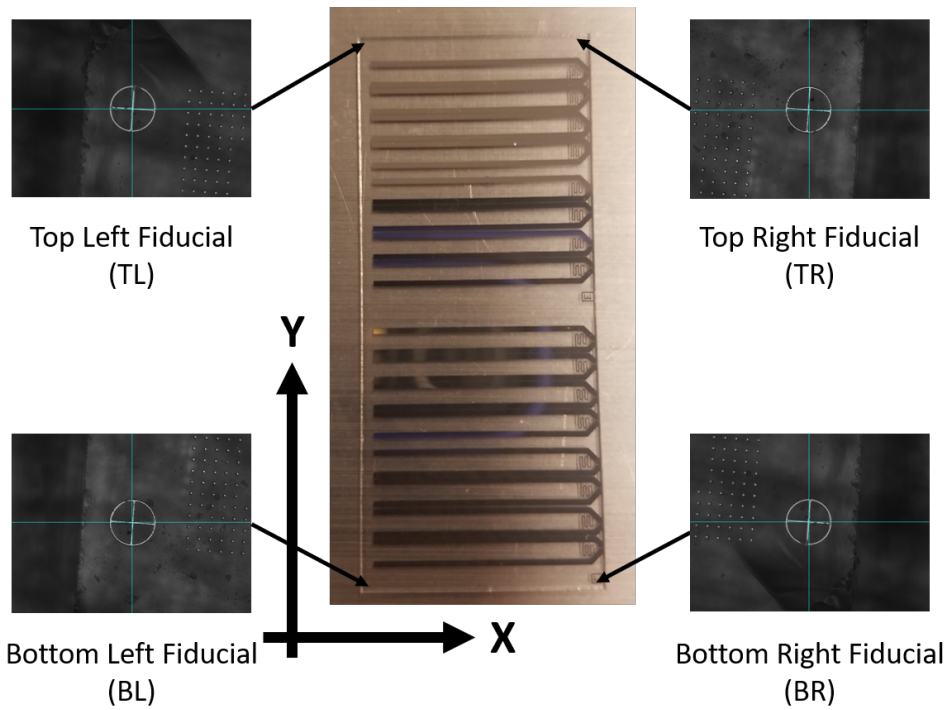

Figure 3.14. The orientation of the coordinate system and features on the thermal mock-up that are recorded to calculate placing accuracy. Henceforth these are referred to as as TL, BL, TR and BR fiducials on the thermal mock-up

Figure 3.15 shows the x-y scatter plots and deviation in x and y of the four fiducials on the mock-up over different iterations.

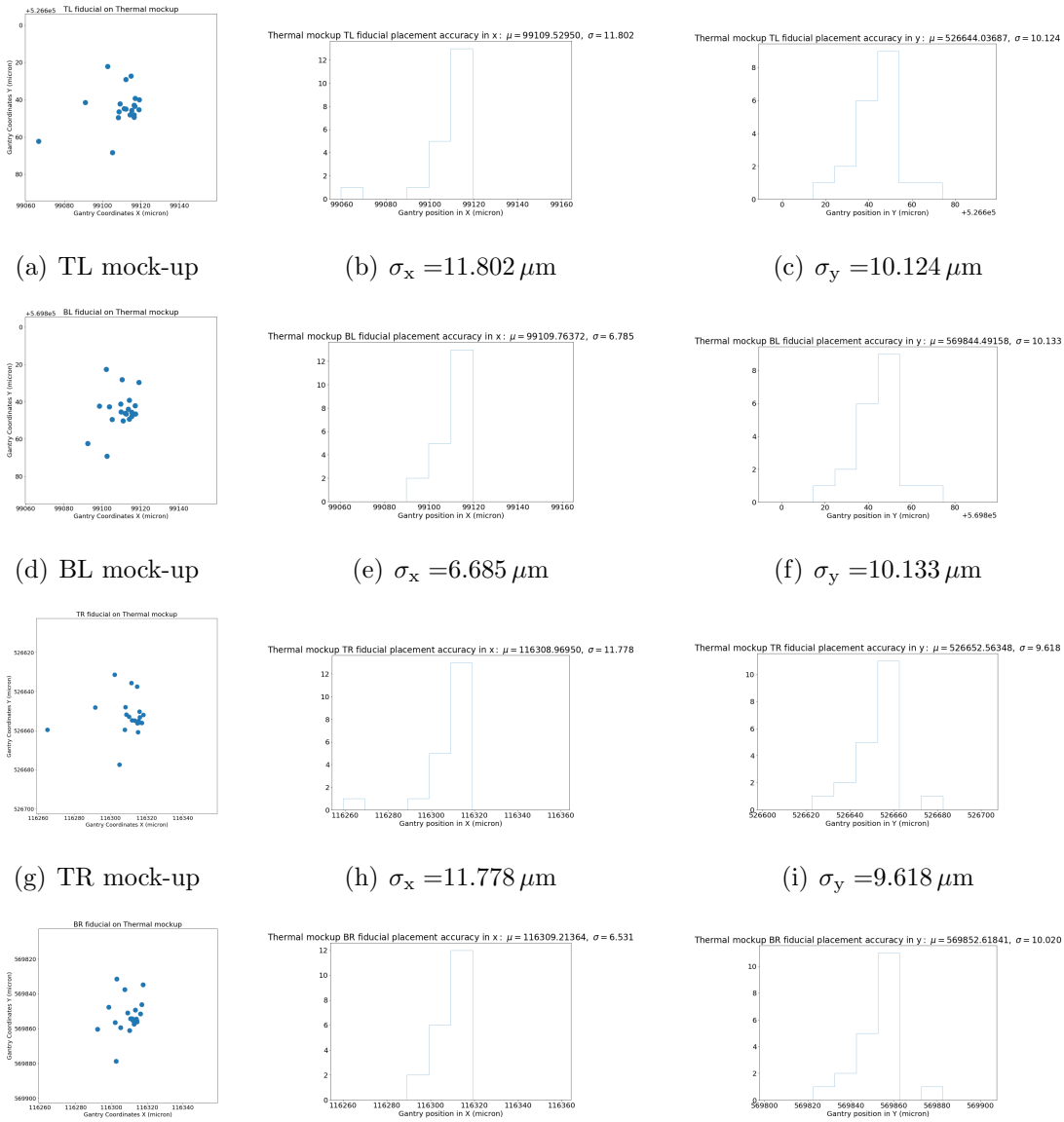

(a) TL mock-up (b) σ_{x} =11.802 μm (c) σ_{y} =10.124 μm

(d) BL mock-up (e) σ_{x} =6.685 μm (f) σ_{y} =10.133 μm

(g) TR mock-up (h) σ_{x} =11.778 μm (i) σ_{y} =9.618 μm

(j) BR mock-up (k) σ_{x} =6.531 μm (l) σ_{y} =10.020 μm

Figure 3.15. Spread of the position of TL, BL, TR, BR fiucials on the thermal mock-up over 10 iterations of alignment with mechanical pins.

The gantry has a precision standard of $\pm 5\mu$m which also factors into this spread. In addition, other variables that needed to be tweaked to achieve this precision are as follows.

- The design of jig and alignment pins must be surveyed. Discrepancies in machining the assembly station parts must be recorded and systematically accounted for. There is LabVIEW code in order to do this calibration.

- Strength of vacuum manifolds must be examined. Because of the layered structure of the assembly station, lack in flatness of any layer can cause a vacuum leak. Screws holding down the vacuum table and assembly tool mitigate this to some extent but a layer of katpon tape may be required between assembly tool and module carrier if there is a leak.

- Speed of tool when picking and placing piece must be observed. Moving too fast around the 1 m x 1 m area can jerk the thermal mock-up in transit. While going up to 50 mm/s is possible across long distances, shorter distances must be traversed slowly. Fast but short windows of movement cause the most jerks. Extremely slow speed and high precision is required between when the tool is a few mm above the mock-up during pick-up so as not to scratch the mock-up or put undue pressure on it. The same caution is required when the mock-up is a few mm above the assembly station before placement. The glass piece must be laid down gently on the assembly station. Besides causing damage, errors in this part of the process can cause placement of the HDI to be offset due to movement while placing.

3.3.2 Glue application and curing

A uniform layer of epoxy is crucial to assembly for both protection radiation hardness and a stiff surface below the bond-pads for wire-bonding. This is not a trivial task and a thin but uniform layer of glue is required. There should be no gaps in the epoxy layer but also no excess that spills over the designated area under the HDI. Spillage can damage the active region of the sensor-ROC assembly. This can be achieved in many ways. Phase I used a stamp tool to get a pattern of uniform dots followed by a weight tool in order to spread out the dots into a uniform layer.

For Phase II, glue application will be done using an epoxy stencil and solder paste spreader. The epoxy stencil also uses dowel pins in assembly fixture for alignment as is shown in Figure 3.16. The solder paste spreader is used to squeegee epoxy over the stencil on to the thermal mock-up.

Figure 3.16. Gluing stencil aligned with mechanical pins and solder paste spreader that is used to squeegee epoxy

This is a much simpler and quicker method yielding similar results. This can be done by the operator without using a precision gantry. However, a gantry tool can be designed to squeegee Araldite 2011 over the stencil. This would involve an attachment to hold the spreader at a fixed angle followed by moving the gantry with tool from one end of the stencil to the other. Uniformity would be achieved by using the same velocity and pressure during glue application. The pattern of glue deposition is the same as Phase I. Figure 3.17 shows the steps of manual glue application.

Araldite as in Phase I takes 24 hours to cure completely. A tool needs to be designed to apply pressure on the HDI once placed while avoiding components on HDI.

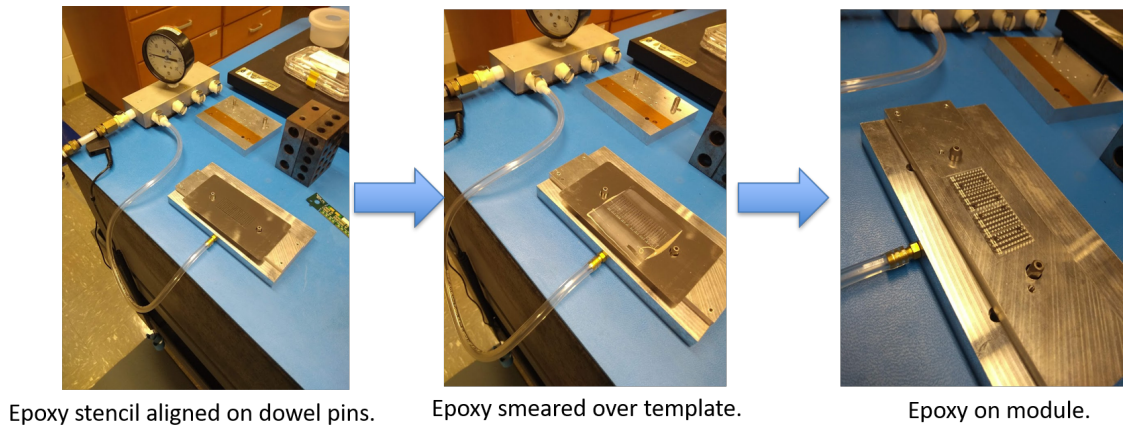

Figure 3.17. Stages of Gluing Process with Stencil

3.4 Encapsulation of Wirebonds

Wire bonding has been used extensively and historically to create interconnections between components during semiconductor device fabrication. There are many methods of wire-bonding using wires made of aluminum, copper, gold and silver. In the CMS Pixel detector wedge bonding of aluminum wires is used to make interconnections between the HDI and sensor-ROC assembly. Wedge bonding is a kind of wire bonding which relies on the application of ultrasonic power and force to form bonds.

The HL-LHC upgrade will use aluminum wire with a diameter of 25 μm. It is proposed to place wire-bonds in a staggered pattern with a pitch of 100 μm, the challenges associated with which are explored in this thesis. These thin and fragile but highly efficient wires need to be encapsulated to provide protection from any transportation and handling damage that may occur between assembly and installation. In addition there is documented evidence of significant electrolytic corrosion that occurs in the detector. [10] The wire-bonds are also exposed to Lorentz resonances that occur as a result of current-carrying wires in a magnetic field as shown in Figure 3.18. As explained in [11], periodic currents if approaching a resonant frequency can amplify

vibrational resonances occurring as a result of Lorentz forces. This eventually stresses the wire at the heel or junction at the feet of bond.

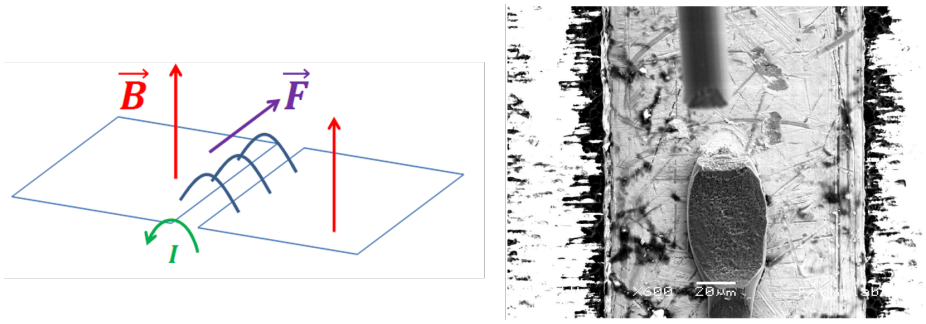

Figure 3.18. Forced harmonic oscillations in the wire bonds can result from currents on some wire bonds in the presence of the 4 T magnetic field used in CMS leading to bond breakage. [11]

This motivates a process of encapsulation which entails covering the feet of wire-bonds with an epoxy in order to increase sturdiness to prevent mechanical damage, neutralize the location where corrosion may occur while increasing mass of the wire-bond in order to dampen the Lorentz vibrational resonances.

3.4.1 Choice of Encapsulant

While the primary goal of the encapsulant is to protect wirebonds, it must also be radiation hard to survive in the HL-LHC. The encapsulant must also have the ability to withstand extreme thermal stress. If the epoxy has a significant coefficient of thermal cycling, too much shrinkage or expansion can cause the wires to break off their connection with the bond-pad. Highly viscous encapsulants are difficult to deposit with extreme precision while low viscosity can lead to the epoxy seeping between the HDI and BBM where it has the potential to damage the active silicon pixel. The encapsulant must also be electrically highly resistive to prevent sparking at high voltage.

Historically, silicone-based Sylgard 186 was used as part of the Phase 0 and I with no problems. In 2018, RD53A single-chip modules were wire bonded at Fermilab and encapsulated with Sylgard. This led to failure after irradiation to 1×10^{16} protons per cm^2. Sylgard appeared to have hardened and cracked and adhesion to module appeared to have failed. The wire bonds were no longer intact possibly due to CTE mismatch. Therefore Sylgard is not considered to be suitable for Phase II TFPX.

This motivated the exploration of other encapsulants and different methods. Resinlab's polyurethane-based UR6060 [12] was investigated for radiation hardness. Phenyl groups present in UR6060 are documented to provide radiation hardness [13]. The UR6060 vs Sylgard 186 coefficient of thermal expansion of was measured at Purdue before and after 235 MRad of gamma radiation at Sandia.

Figure 3.19. Sylgard 186 vs UR6060 before and after 235 MRad of gamma radiation at Sandia

Sylgard 186 came back brittle, difficult to peel off glass without shattering. UR6060 came back unchanged, with slightly lower CTE. UR6060 is also less viscous than Sylgard 186. Additionally, fewer bubbles are formed over the curing process of UR6060. This is shown in Figure 3.19. Given these motivations, the following section explores the methods of encapsulation using UR6060.

3.4.2 Method of Encapsulation

The method of encapsulating can be broadly broken into mixing the encapsulant, calibrating the needle tip and finally, depositing the encapsulant.

Mixing of Encapsulant

UR6060 Clear is a clear, colorless two-part (A & B) polyurethane. Part A and B need to be mixed in a 1:1 ratio by volume. If encapsulant is mixed with a sufficiently long mixing tube it does not need to be centrifuged. If the mixing tube is not long enough, the mixture will appear separated and stringy. If mixed by hand, UR6060 needs to be mixed till there is no visible separation between the two liquids which is hard to observe because of all the bubbles formed when mixing manually. To ensure complete mixing, it is recommended to use a mixing tube with 20 or more mixing points and maintain an adequate velocity during dispensing through the tube. If manual mixing is unavoidable, it is recommended to mix for two minutes continuously and centrifuge for 3 minutes after.

Once mixed, the encapsulant needs to be loaded into the syringe. This can be achieved easily using the mixing tube and applying a reasonable and steady pressure to fill the syringe. A centrifuge may be used to remove any bubbles formed, however this is a factor that can reduce the pot life of UR6060.

To ensure consistency across production sites, it is recommended to use a side-by-side cartridge format with attached mixing tube during production as shown in Figure 3.20(a). Mixing quality affects deposition parameters and can be visually seen as in Figure 3.20(b).

Needle Tip Offset Calibration

An ESD safe 33 gauge needle tip was used to deposit encapsulant. Each needle tip needs to be calibrated before being used to encapsulate and is done with the following

(a) ResinLab UR6060 side-by-side cartridge with attached mixing tube

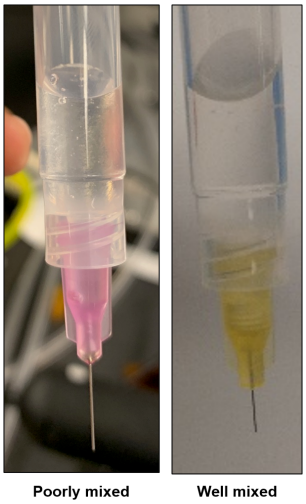

(b) Results of mixing

Figure 3.20. Encapsulant Mixing

mechanism: Firstly, once a new needle tip is attached to the newly loaded syringe, it must be "purged" to allow the encapsulant to load the new tip and remove any air gaps near the tip.

Then the syringe is loaded into the dispensing tool. Using the gantry camera, calibration set-up cameras and a calibration needle, the new tip is calibrated. The two steps for this calibration are:

1. Align the dispenser needle with calibration needle using the gantry. Check alignment with stand camera.

2. Gantry head camera moved to see calibration needle from above

Difference between positions from step 1 & 2 as shown in 3.21(b) is the offset between the camera and needle tip.

This makes it possible to accurately dispense encapsulant to a precise location that the vision system of the gantry can locate.

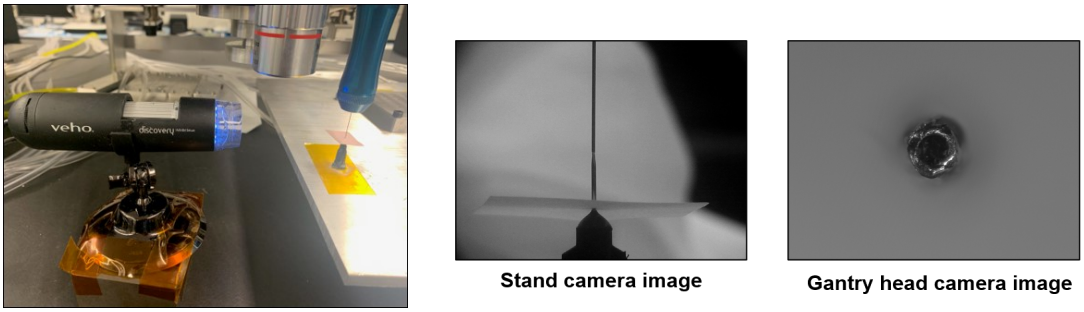

(a) Offset Calibration Setup

(b) Step 1 & 2 of Calibration

Figure 3.21. Needle Tip Offset Calibration

Depositing Encapsulant

For each type on needle-tip used in encapsulation, the width of a deposited line of UR6060 depends on the three parameters; time after mixing (t), speed of needle (v) and pressure in dispenser (P). The phase space of these parameters is explored by depositing lines at different P,v and t and measuring the width attained.

UR6060 doubles in viscosity in the first 15 minutes and will cure within 6 hours at room temperature. At time of mixing, it has a liquid consistency that changes to a gel in the first 15-20 minutes. This gel can still be deposited effectively for a total of 90 minutes from mixing. This time can be extended with a different needle gauge but changing needle tips during deposition is not an easy task that can be repeated accurately.

The effect of pressure and velocity on the encapsulant are characterized independently. The width of the line varies much more with respect to velocity than pressure as is seen in the figure. Hence, fixing pressure and varying velocity provides more control on the width of line deposited for a given time range.This is also compatible with the hardware setup as velocity of the gantry is easier to manipulate in real time than is the pressure of the EFD dispensing system.

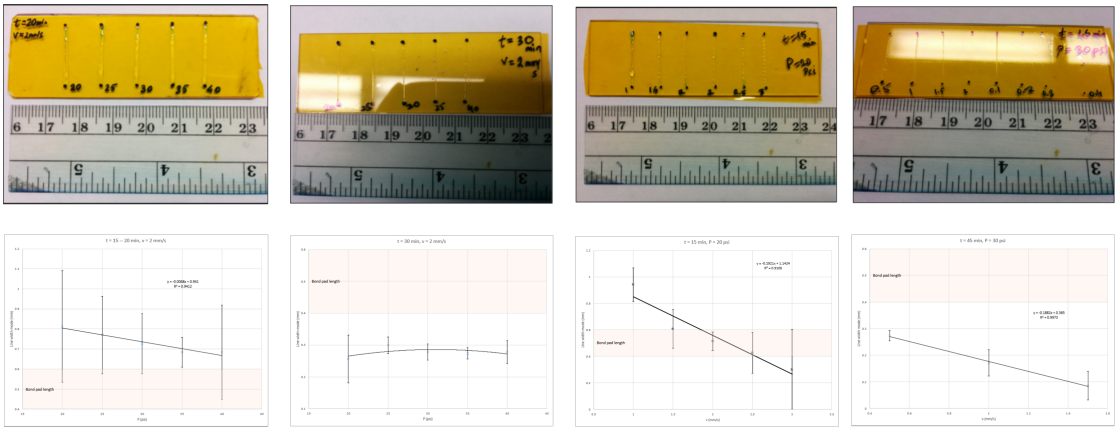

(e) 15 min, v = 2 mm/s (f) 30 min, v = 2 mm/s (g) 15 min, P = 20 psi (h) 45 min, P = 30 psi

Figure 3.22. Effect of velocity and pressure on line width measured independently

Fixing pressure and velocity, a long snake patterned line is deposited on a glass piece in intervals of 600 s and the date plotted in Figure 3.23. It is now clear that while there is an overall downward trend, extended pressure on the encapsulant for 600 s also has a trend of its own.

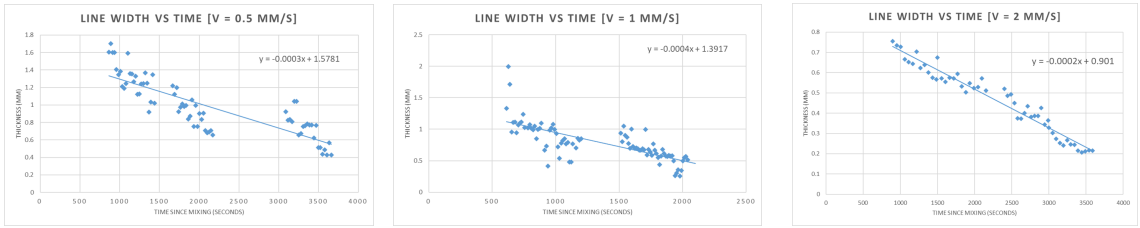

(a) Velocity = 0.5 mm/s (b) Velocity = 1 mm/s (c) Velocity = 2 mm/s

Figure 3.23. Velocity dependence at a fixed P = 20 Psi

Putting together all this data yields a formula (3.1) that characterizes to some degree a good starting point to work with UR6060 at a pressure of 20 Psi as shown in Figure 3.24.

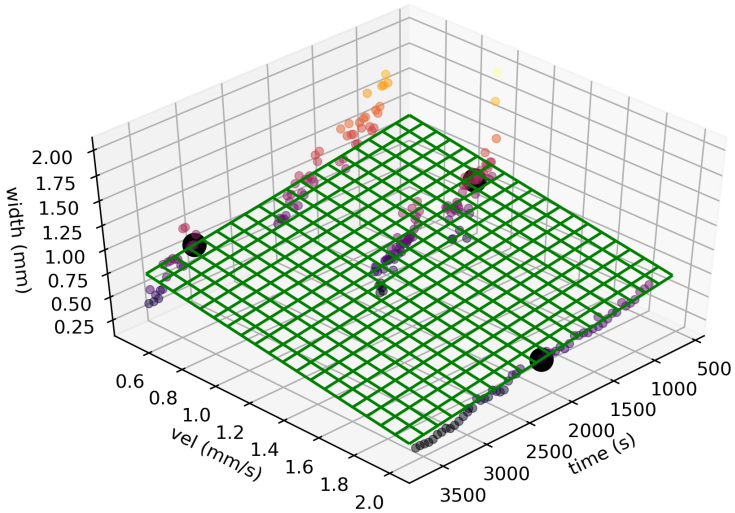

Figure 3.24. Width dependence on Velocity and Time at a Pressure of 20 Psi

$$0.4 \times t + 877.5 \times v + 2900.5 \times w = 4132.5 \tag{3.1}$$

However, it is also increasingly clear that while there are optimal ranges for dispensing of UR6060, it is in-fact very difficult to formulate the exact velocity and time relationship to get a specific width. Equation 3.3 shows for example the velocity to be used for 0.5 mm width for the HDI bond-pad and 0.3 mm width for the module bond-pad.

$$w = 0.5mm, v = 3.056 - 0.00047 \times t \tag{3.2}$$

$$w = 0.3mm, v = 3.718 - 0.00047 \times t \tag{3.3}$$

Problem of Staggered Wire-bonds

While it is not the decided design of wire-bonds for Phase II, staggered bonds are the current proposed solution to increase the density of connections required to

increase granularity of the detector. This would require encapsulant to be deposited on a staggered wire-bonding configuration as shown in Figure 3.25

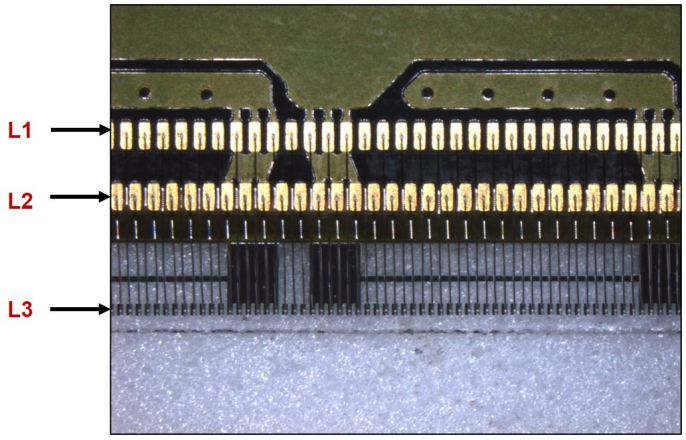

Figure 3.25. Staggered Bonds showing short (L2 to L3) and long (L1 to L3) wire-bonds

A few different methods to achieve this are explored with varying degrees of success. Firstly, line encapsulation of L1, L3 and drop encapsulation of L2.

This requires squeezing the dispenser needle in between bonds which is very challenging given the size of the needle and pitch of wire-bonds as shown in Figure 3.26(a). While possible, this method is not efficiently reproducible. This involves calibrating exact time after cure and pressure to deposit perfect drop. Slight misalignment can damage wire-bonds as shown in Figure 3.26(b) and also leave exposed bond-pads (Figure 3.26(c))

Another option is to first wire-bond the short bonds, encapsulate L2 followed by the long wire-bonds and encapsulation of L1 and L3. This is possible with accurately deposited lines but the two-step wire-bonding is still being developed. Additionally, this method requires re-calibration of local coordinates between assembly & wire bonding stations which requires additional operator time and some possible alignment error.

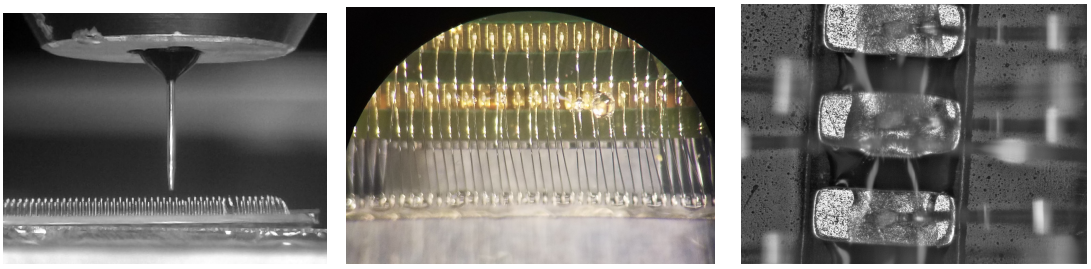

(a) Guiding needle between bonds is very hard (b) Slight misalignment can push down longer wire-bonds (c) Drops often leave exposed bond-pad

Figure 3.26. Problems that occurred while dropping encapsulant

A third possibility is to only encapsulate L1 & L3. This was achieved successfully as is shown in Figure 3.27. The added mass of encapsulant does greatly reduce vibration in the magnetic field. These samples were sent for irradiation to see radiation damage.

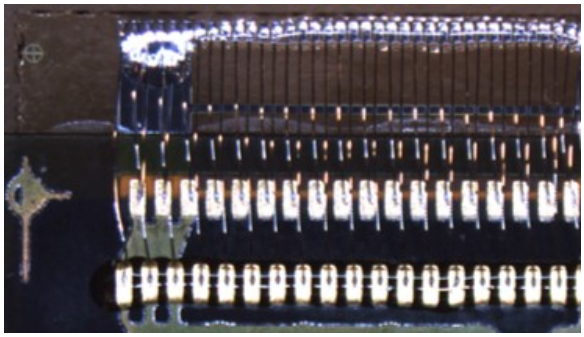

Figure 3.27. Successful Encapsulation of L1 and L3

3.4.3 Irradiation Effects

Three encapsulated modules with L1 and L3 successfully encapsulated were sent to a Sandia irradiation campaign of 90 ± 18 MRad. This is a much lower dose than the 1 GRad that will be used to test radiation hardness for the HL-LHC but was

used as a preliminary check for the radiation hardness of UR6060. There was no preliminary damage as is shown in Figure 3.28. This confirmed that UR6060 is at least as rad-hard as Sylgard 186 but future irradiation campaigns are needed to test it to the required dose.

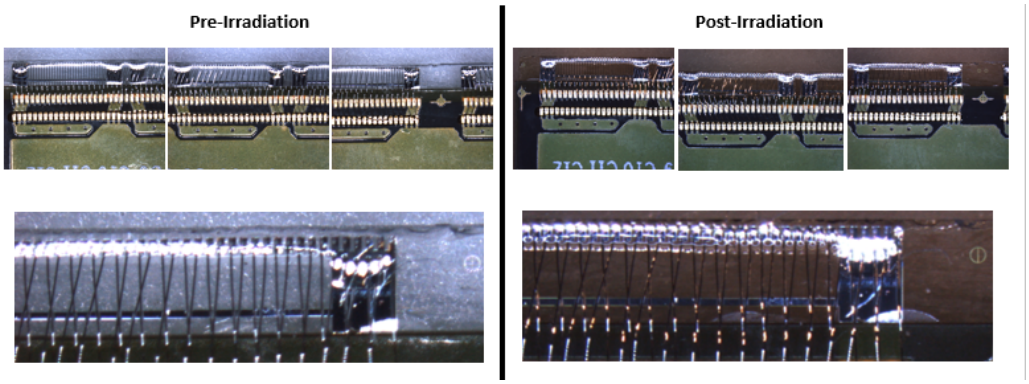

Figure 3.28. Encapsulated module pre and post 90 ± 18 MRad Sandia Irradiation

4. CONCLUSION

4.1 Results & Discussions

The labview code developed for Phase-II assembly has been developed and tested to successfully to avoid memory leaks. The GUIs are designed with a uni-directional workflow and manuals to aid in learning and operation. The code also successfully translates across assembly sites. The accuracy attained by mechanical pins and use of the Aerotech precision gantry is within $20\,\mu m$ which is the required order of magnitude set for this iteration of assembly routines. Encapsulation with UR6060 while attainable gives a very short window for encapsulation. It also shows that while the exploration of the phase space described by speed, pressure and time from mixing of UR6060 yields a formula for a good starting point, a fair amount of experience is required to make changes in real time to encapsulate successfully. However, it is shown to outperform Sylgard 186 in preliminary radiation tests and hence still the choice of encapsulant for Phase-II.

4.2 Future Work

While the pick-and place procedures have now been established with repeat-ability, the next steps include ensuring this can be repeated across different mock-pieces and account for manufacturing defects. It is also important to have different individuals run the routines to ensure the accuracy can be maintained irrespective of operator. The limited encapsulation window motivates the investigation of spraying polyurethane as is explored in [14]. If adapted to fit the Phase-II module assembly routine, it can be evaluated for efficiency over syringe deposition.

REFERENCES

[1] Stella Orfanelli. Pixel detector for CMS upgrade. *Tribology International*, 16(5):277–279, 1983.

[2] Lyn Evans. Lhc machine. page 004, 2008.

[3] Giovanni Petrucciani and Giovanni Petrucciani. The CMS experiment at the CERN LHC. *The Search for the Higgs Boson at CMS*, pages 15–58, 2013.

[4] E Daw. Lecture 7 - Rapidity and Pseudorapidity. *Lecture Notes*, pages 1–8, 2012.

[5] O Stein, A Infantino, C Bahamonde Castro, L Esposito, A Ciccotelli, and M Mendes. Radiation level specifications for HL-LHC. 2019.

[6] Mayur Babna. Development of ultra radiation-hard silicon sensors for high luminosity upgrade of LHC. 2015.

[7] D Abbaneo, Jim (Cornell University) Alexander, P Azzi, E Brondolin, A Canepa, J Christiansen, S Costa, A Dabrowski, C Delaere, A Dierlamm, M Dragicevic, R Fruhwirth, K Hahn, A Honma, K Klein, S Mersi, A Mussgiller, M Narain, A Onnela, G Sguazzoni, G Steinbrueck, Julia (Cornell University) Thom-Levy, A Tricomi, F Vasey, and Peter (Cornell University) Wittich. The Phase-2 Upgrade of the CMS Tracker - Technical Design Report. *CERN - CMS Collaboration*, (June), 2017.

[8] Lea Caminada. Recent Developments of HEP Pixel Detector Readout Chips. *Physics Procedia*, 37:1644–1653, 2012.

[9] Simran Gurdasani. forked repository of original pixel-gantry-control software. `https://github.com/sgurdasa/pixel-gantry-control`, 2019.

[10] Douglas R. Sparks. Chemically-accelerated corrosion tests for aluminum metallized ICs. *Thin Solid Films*, 235(1-2):108–111, 1993.

[11] G. Bolla, M. Atac, V. Pavlicek, G. Cancelo, S. Nahn, R. Mumford, M. Garcia-Sciveres, T. Nguyen, S. Forrester, C. Hill, J. Olszewski, A. Rahaman, J. Goldstein, B. Ashmanskas, T. Maruyama, R. S. Lu, J. Spalding, Z. Tang, T. Zimmerman, S. Moccia, and J. D. Lewis. Wire-bonds failures Induced by resonant vibrations in the CDF silicon detector. *IEEE Nuclear Science Symposium Conference Record*, 3:1641–1645, 2003.

[12] N W and Ellsworth Drive. eleset TM UR6060 Clear Technical Data Sheet eleset TM UR6060 Clear Technical Data Sheet. pages 3–5, 2018.

[13] A. A. Miller. Effects of High-Energy Radiation on Polymers. *Annals of the New York Academy of Sciences*, 82(3):774–781, 1959.

[14] J. M. Izen, M. Kurth, and R. Boyd. Polyurethane spray coating of aluminum wire bonds to prevent corrosion and suppress resonant oscillations. *Journal of Instrumentation*, 11(3), 2016.